AD-A094 233 PACIFIC-SIERRA RESEARCH CORP SANTA MONICA CA F/G 17/7
AN INTEGRAL EQUATION APPROACH TO THE PROPAGATION OF LOW-FREQUEN--ETC(U)
NOV 80 S GAYER, E C FIELD, B D'AMBROSIO F19628-78-C-0088
UNCLASSIFIED PSR-929 RADC-TR-80-334 NL

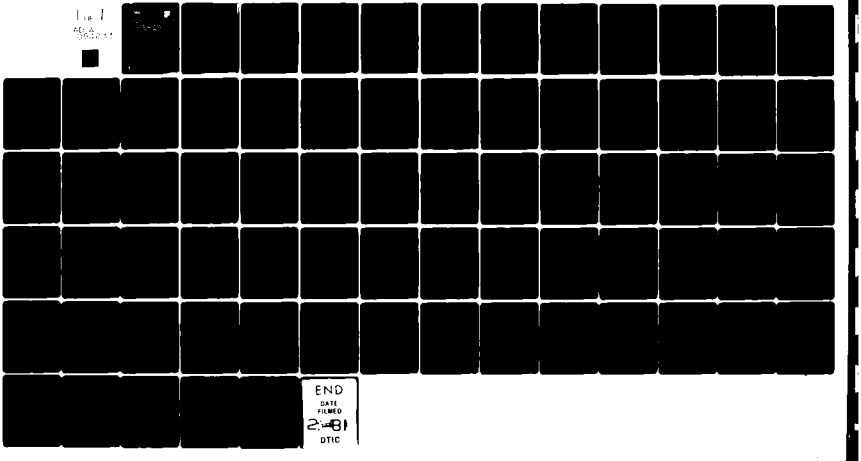

END
DATE FILMED
2-81
DTIC

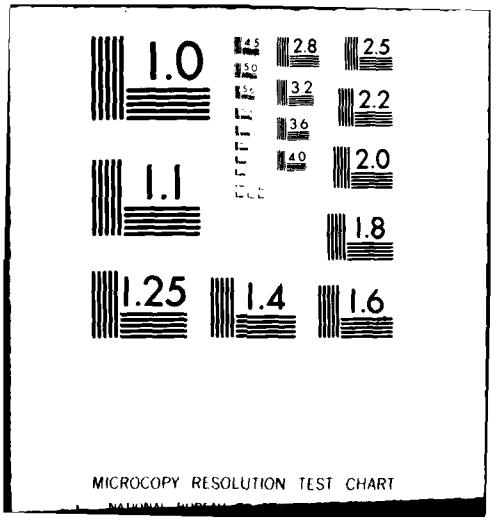
1.0
1.1
1.25
1.4
1.6
1.8
2.0
2.2
2.5
2.8
3.2
3.6
4.0
4.5
5.0
MICROCOPY RESOLUTION TEST CHART

RADC-TR-80-334
Interim Report, Apr 78 - Oct 79
Nov 1980

LEVEL II

AN INTEGRAL EQUATION APPROACH TO THE PROPAGATION OF LOW-FREQUENCY GROUND WAVES OVER IRREGULAR TERRAIN: I. GROUND-BASED TERMINALS

Pacific-Sierra Research Corp.

S./Geyer
E. C. Field, Jr.
B./D'Ambrosio

PSR-929

DTIC
ELECTE
JAN 28 1981
S D
E

F19628-78-C-0088

2344
J3

ROME AIR DEVELOPMENT CENTER
Air Force Systems Command
Griffiss Air Force Base, New York 13441

This report has been reviewed by the RADC Public Affairs Office (PA) and is releasable to the National Technical Information Service (NTIS). At NTIS it will be releasable to the general public, including foreign nations.

RADC-TR-80-334 has been reviewed and is approved for publication.

APPROVED: Paul A. Kossey

PAUL A. KOSSEY
Project Engineer

APPROVED: Allan C. Schell

ALLAN C. SCHELL, Chief
Electromagnetic Sciences Division

FOR THE COMMANDER: John P. Huss

JOHN P. HUSS
Acting Chief, Plans Office

If your address has changed or if you wish to be removed from the RADC mailing list, or if the addressee is no longer employed by your organization, please notify RADC (EEP) Hanscom AFB MA 01731. This will assist us in maintaining a current mailing list.

Do not return this copy. Retain or destroy.

UNCLASSIFIED

SECURITY CLASSIFICATION OF THIS PAGE (When Data Entered)

REPORT DOCUMENTATION PAGE		READ INSTRUCTIONS BEFORE COMPLETING FORM
1. REPORT NUMBER RADC-TR-80-334	2. GOVT ACCESSION NO.	3. RECIPIENT'S CATALOG NUMBER
4. TITLE (and Subtitle) AN INTEGRAL EQUATION APPROACH TO THE PROPAGATION OF LOW-FREQUENCY GROUND WAVES OVER IRREGULAR TERRAIN: I. GROUND-BASED TERMINALS		5. TYPE OF REPORT & PERIOD COVERED Interim Report Apr 78 - Oct 79 6. PERFORMING ORG. REPORT NUMBER PSR Report 929
7. AUTHOR(s) S. Gayer E. C. Field, Jr. B. D'Ambrosio		8. CONTRACT OR GRANT NUMBER(s) F19628-78-C-0088
9. PERFORMING ORGANIZATION NAME AND ADDRESS Pacific-Sierra Research Corp 1456 Cloverfield Blvd Santa Monica CA 90404		10. PROGRAM ELEMENT, PROJECT, TASK AREA & WORK UNIT NUMBERS 61102F 2304J322
11. CONTROLLING OFFICE NAME AND ADDRESS Deputy for Electronic Technology (RADC/EEP) Hanscom AFB MA 01731		12. REPORT DATE November 1980 13. NUMBER OF PAGES 73
14. MONITORING AGENCY NAME & ADDRESS(if different from Controlling Office) Same		15. SECURITY CLASS. (of this report) UNCLASSIFIED 15a. DECLASSIFICATION/DOWNGRADING SCHEDULE N/A

16. DISTRIBUTION STATEMENT (of this Report)

Approved for public release; distribution unlimited.

17. DISTRIBUTION STATEMENT (of the abstract entered in Block 20, if different from Report)

Same

18. SUPPLEMENTARY NOTES

RADC Project Engineer: Paul A. Kossey (RADC/EEP)

19. KEY WORDS (Continue on reverse side if necessary and identify by block number)

Ground wave
LORAN
Low-Frequency propagation

20. ABSTRACT (Continue on reverse side if necessary and identify by block number)

Developing a highly accurate method of predicting the arrival time of a LORAN pulse traveling as a ground wave, this report considers the one dimensional integral-equation method of analyzing propagation over irregular terrain. Numerical calculations and theoretical developments demonstrate how topography and various approximations affect the calculated propagation of a ground wave. We find that curvature effects entering through geometric terms of the integral equation for the —> cont'd.

(Cont'd)

DD FORM 1 JAN 73 1473 EDITION OF 1 NOV 65 IS OBSOLETE

UNCLASSIFIED

SECURITY CLASSIFICATION OF THIS PAGE (When Data Entered)

Item 20 (Cont'd)

propagation of phase work strongly, but that those entering through a modified impedance condition are insignificant. Dispersion of the pulse can cause cycle ambiguity in the signal. For a ground conductivity of 0.001 mho/m, cycle ambiguity appears at a distance from the transmitter of roughly 1500 km.

Extensive numerical results are presented for generic terrain types selected to illustrate salient features of solutions to the integral wave equation. Results for simple hills show that arc-length correction of the propagation path is insignificant compared with geometric effects on phase speed in predicting phase retardation. Isolated terrain features cause large local perturbations in phase arrival; far beyond the irregularity on the propagation path, effects are observable but diminish with distance. The one dimensional version of the integral wave equation can overstate the effect of terrain features that are localized in the direction transverse to the great-circle propagation path.

SUMMARY

Developing a highly accurate method of predicting the arrival time of a LORAN pulse traveling as a ground wave, this report considers the one-dimensional integral-equation method of analyzing propagation over irregular terrain. Numerical calculations and theoretical developments demonstrate how topography and various approximations affect the calculated propagation of a ground wave. We find that curvature effects entering through geometric terms of the integral equation for the propagation of phase work strongly, but that those entering through a modified impedance condition are insignificant. Dispersion of the pulse can cause cycle ambiguity in the signal. For a ground conductivity of 0.001 mho/m, cycle ambiguity appears at a distance from the transmitter of roughly 1500 km.

Extensive numerical results are presented for generic terrain types selected to illustrate salient features of solutions to the integral wave equation. Results for simple hills show that arc-length correction of the propagation path is insignificant compared with geometric effects on phase speed in predicting phase retardation. Isolated terrain features cause large local perturbations in phase arrival; far beyond the irregularity on the propagation path, effects are observable but diminish with distance. The one-dimensional version of the integral wave equation can overstate the effect of terrain features that are localized in the direction transverse to the great-circle propagation path.

PREFACE

This report continues Pacific-Sierra Research Corporation's (PSR) analysis of ground wave propagation, specifically the effort to develop a highly accurate method of predicting LORAN coordinates over irregular terrain. In an earlier report, Field and Allen determined which approximations in the chosen mathematical treatment have an important effect on accuracy, and discussed their significance.*

The present report continues the analysis of Field and Allen, and determines the numerical consequences of the approximations they treated. In three essentially independent analyses, this report evaluates the importance of the effect of ground curvature on ground impedance; defines the distances over which group effects modify the arrival time of a LORAN pulse; and presents numerical results obtained from PSR's developing propagation code, which will handle arbitrary ground data and has been completed for the case of terminals on the ground. The PSR ground-wave-propagation code can be incorporated into a LORAN map-making program. An analysis of the continuity of solutions for ground-based and low-elevation receivers is included as an appendix; numerical methods for dealing with elevated receivers will be addressed in a later phase of this analysis.

---

*E. C. Field and R. Allen, *Propagation of the Low-Frequency Groundwave over Nonuniform Terrain*, Rome Air Development Center, RADC-TR-78-68, March 1978.

CONTENTS

SUMMARY iii

PREFACE v

FIGURES ix

TABLES xi

Section
I. INTRODUCTION 1

II. CURVATURE CORRECTIONS TO SURFACE IMPEDANCE CONDITION . 3

III. TIME OF ARRIVAL OF THIRD-CYCLE ZERO CROSSING 8
Method of Analysis 9
Conclusions 14

IV. NUMERICAL STUDIES OF SURFACE PHASE PROPAGATION 18
Smooth Earth 20
Terrain on Flat Earth 22
Simple Ramp Terrain 22
Continuous-Slope Terrain 29
Terrain on Round Earth 32
Hills 32
Valleys 35
Hill and Valley Combinations 37
Minimum Significant Terrain Feature 37
Conclusions 41

REFERENCES 45

Appendix
A. DERIVATION OF CURVATURE CORRECTION TO SURFACE IMPEDANCE 47
B. CALCULATION OF LORAN SPECTRAL INTENSITY FUNCTION 54
C. CONSISTENCY OF HEIGHT GAIN FUNCTION FORMULATIONS AT FLAT PLANE SURFACE 59

SYMBOLS 63

FIGURES

1. Geometry for Calculation of Surface Impedance with Curvature Correction 5
2. Physical Interpretation of Surface Impedance Correction 7
3. Arrival Times Associated with LORAN Pulse 10
4. Spectral Distribution of Transmitted Pulse 15
5. Amplitude of Transfer Function of LORAN Pulse at 76 and 3076 km for Ground Conductivity 0.01 mho/m 16
6. Amplitude of Transfer Function of LORAN Pulse at 76 and 3076 km for Ground Conductivity 0.001 mho/m 17
7. Geometrical Relationships among Various Distances in Integral Equations (12) and (13) 19
8. Amplitude and Phase of W for Smooth, Flat Earth of Conductivities 0.01 and 0.001 mho/m 21
9. Phase of W for Smooth, Round Earth of Conductivities 0.01 and 0.001 mho/m with No Correction for $(i/kr_2)(\partial r_2/\partial n)$ 21
10. Phase of W for Smooth, Round Earth Minus Phase of W for Smooth, Flat Earth 22
11. Phase Differences for Several Constant Slopes Beginning at 50 km, with No Correction for $(i/kr_2)(\partial r_2/\partial n)$ 24
12. Phase Difference for Ramp of Slope 0.3 Beginning at 50 km, with and without Correction for $(i/kr_2)(\partial r_2/\partial n)$. 24
13. Phase Difference for Ramps of Slopes -0.1 and -0.3, Both Beginning at 50 km 26
14. Phase Difference for Ramps of Slopes -0.1 and 0.1, Both Beginning at 50 km 26
15. Amplitude of W for Ramps of Slopes 0.3 and -0.3 27
16. Phase Difference for Ramp Beginning at 50 km that Changes Slope from 0.1 to 0.2 at 100 km 28
17. Phase Difference for Ramp Beginning at 50 km that Changes Slope from 0.1 to 0.05 at 100 km 28
18. Phase Difference for Pyramid Beginning at 50 km with Faces of Slopes 0.1 and -0.1 (characteristic signature of symmetrical hill) 30
19. Phase Difference for $1 \times 10 \sin^2$ Hill Beginning at 50 km, with and without Correction for $(i/kr_2)(\partial r_2/\partial n)$. 31
20. Phase Difference Plot Comparing 1×10 Pyramid with $1 \times 10 \sin^2$ Hill, Both Beginning at 50 km 31

21. Phase Difference for 1 × 10 $\sin^2$ Hill Beginning at 50 km, with Conductivities 0.01 and 0.001 mho/m 33

22. Phase Differences for Three Different $\sin^2$ Hills Beginning at 50 km 33

23. Phase Differences for 1 × 10 $\sin^2$ Hills Beginning at 5, 110, and 400 km 34

24. Geometry of Hills Near and Far from Transmitter 35

25. Phase Difference Plot Comparing 1 × 10 $\sin^2$ Hill and Valley, Both Beginning at 50 km 36

26. Phase Difference for 1 × 50 $\sin^2$ Valley Beginning at 50 km 38

27. Phase Difference Plot Comparing 7.5 × 25 $\sin^2$ Hill and Valley, Both Beginning at 50 km 38

28. Phase Difference for 1 × 10 $\sin^2$ Hill Beginning at 50 km, Followed by 1 × 10 $\sin^2$ Valley Beginning at 70 km 39

29. Phase Difference for 1 × 10 $\sin^2$ Valley Beginning at 50 km, Followed by 1 × 10 $\sin^2$ Hill Beginning at 70 km 39

30. Phase Difference for 1 × 10 $\sin^2$ Hill Beginning at 50 km, Followed by 1 × 10 $\sin^2$ Valley Beginning at 90 km 40

31. Phase Difference for 1 × 10 $\sin^2$ Valley Beginning at 50 km, Followed by 1 × 10 $\sin^2$ Hill Beginning at 90 km 40

32. Phase Difference for Sequence of Two 0.5 × 5 $\sin^2$ Hills 42

33. Phase Difference for Sequence of Four 0.25 × 2.5 $\sin^2$ Hills 42

34. Phase Difference for Sequence of Ten 0.1 × 1.0 $\sin^2$ Hills 43

TABLES

1. Spread Factors and Propagation Velocities for Ground Conductivity of 0.01 mho/m at Several Distances 13

2. Spread Factors and Propagation Velocities for Ground Conductivity of 0.001 mho/m at Several Distances 13

I. INTRODUCTION

LORAN navigation depends on the determination of arrival times of pulses centered in frequency at 100 kHz. Electrical and topographical variations along the propagation path can, however, considerably influence such arrival times. Pacific-Sierra Research Corporation (PSR) is developing a numerically efficient method of predicting ground wave propagation over irregular terrain that most nearly satisfies two conflicting goals: (1) achieving the highest precision commensurate with the 2.5 nsec resolution of modern receivers (Fehlner et al. [1973]) while (2) incorporating general electrical and topographical ground characteristics.

Virtually exact analyses reported previously (e.g., Norton [1937]) are valid only for flat or smooth, spherical surfaces. The one-dimensional integral-equation approach used here accommodates a great variety of conductivity and topographical features, provided they are not too abrupt. One version of this method has been explored by Johler and Berry [1967]. Our approach uses different numerical techniques and considers in greater depth several important aspects of LORAN pulse propagation for ground-based terminals. The integral equation approach involves several approximations; however, careful handling of certain terms permits reasonable accuracy, as discussed by Field and Allen [1978].

This report extends the analysis of Field and Allen, and determines the numerical consequences of the approximations they treated. Section II examines the impedance boundary condition. Previously, the only definitive treatment of curvature effects on ground impedance was that of Rytov [1940]. Unfortunately, his analysis is available only in Russian; furthermore, application of Rytov's formulas requires ground surface data to be in an impractical form--given by the metric in an arbitrary set of curvilinear coordinates molded to the surface. Thus Rytov obfuscates physical interpretation of his conclusion. We have reexamined the problem using the same physical assumptions, substituting an equivalent but more practical description of the surface.

Section III examines dispersion of the multiple-component LORAN pulse, which cannot be treated exactly by the ground-wave integral equation useful for monochromatic waves. In the absence of dispersion, that equation can be applied directly to the propagation of the LORAN pulse. In the presence of dispersion, however, it can only *approximately* predict the time of arrival of some physical property of the pulse--e.g., a zero crossing--because such properties can no longer be exactly identified with phase. If the pulse were nearly monochromatic, the approximation would be very good.

LORAN receivers typically use a particular zero crossing as the arrival time of the pulse. However, calculations of arrival time are usually based on carrier phase. Our analysis shows that a LORAN pulse is sufficiently monochromatic that a specified zero crossing can be closely approximated by a specified point of the carrier phase, provided the range is not too great. Nevertheless, since we find that zero crossings traverse the pulse envelope, there is a range beyond which the number of a particular zero crossing is ambiguous.

Section IV presents numerical results for ground-based terminals. To illustrate the effect of generic terrain features on the phase of a 100 kHz sinusoidal signal, we consider a succession of models beginning with smooth ground, then proceeding to increasingly complicated structures--i.e., a flat, sloping ramp inclined with respect to smooth ground; a ramp whose sections have different slopes; and a pyramid-shaped hill consisting of two equal-length ramps. Simple sets of ramps can be constructed to yield virtually the same phase behavior caused by any more complicated ground shape. For example, the pyramid's effect on phase has a signature typical of any simple hill of similar height and width.

Section IV also considers combinations of hills and valleys on a round earth, varying their size, shape, number, spacing, and location. The numerical importance of certain mathematical terms is evaluated.

Appendixes A, B, and C present derivations of the curvature impedance, the LORAN spectral distribution, and the analytical continuity of height gain at the ground surface, respectively.

II. CURVATURE CORRECTIONS TO SURFACE IMPEDANCE CONDITION

In discussing curvature terms in the surface impedance formula, previous wave propagation analyses [Senior, 1961; Leontovich, 1944] refer ultimately to the calculation of Rytov [1940]. Rytov's calculation, though quite elegant, is not easily applied to real terrain since it assumes that the metric is given for the surface over which propagation is considered. Curvilinear coordinates are then employed to calculate a curvature correction from derivatives of the logarithm of metric component ratios.

Rytov's method simplifies the problem in the abstract, but complicates the solution of concrete cases. However, using a straightforward formalism, we can find a more practical solution to the same problem. To do so, we rederive curvature corrections using cartesian coordinates, MKS units, and the following physical assumptions employed by Rytov:

- We can neglect the displacement current in the medium over which the waves are propagating.
- The index of refraction is large enough that Snell's law gives propagation nearly normal to the surface of the conductor.
- The skin depth in the medium is small relative to characteristic radii of curvature, so we may expand the electric field in a power series of the ratio of skin depth to radii of curvature.

We outline here the method of calculating the first curvature correction to the surface impedance condition; Appendix A contains a detailed derivation. The calculation begins by solving the following two Maxwell electromagnetic field equations:

$$\nabla \times \vec{E} = -\mu \frac{\partial \vec{H}}{\partial t} , \tag{1}$$

$$\nabla \times \vec{H} = \sigma \vec{E} , \tag{2}$$

where, expanding the electric field $\vec{E}$ and the magnetic intensity $\vec{H}$,

$$\vec{E} = (\vec{E}_0 + \delta\vec{E}_1 + \delta^2\vec{E}_2 + \cdots) \exp\left\{ i\left[\frac{\psi(x, y, z)}{\delta} - \omega t\right]\right\} , \tag{3}$$

$$\vec{H} = (\vec{H}_0 + \delta\vec{H}_1 + \delta^2\vec{H}_2 + \cdots) \exp\left\{ i\left[\frac{\psi(x, y, z)}{\delta} - \omega t\right]\right\} , \tag{4}$$

and the skin depth δ is given by

$$\delta = \left(\frac{2}{\omega\sigma\mu}\right)^{\frac{1}{2}} , \tag{5}$$

and where σ is ground conductivity, measured in mhos per meter; μ is permeability; t is time; ψ is the phase; and ω is the frequency.

The condition of normal propagation is applied by defining three vectors, $\vec{A}$, $\vec{B}$, and $\vec{n}$, where $\vec{A}$ and $\vec{B}$ are orthonormal vectors tangent to the conductor and $\vec{n}$ is the unit normal into the conductor so that $\vec{A} \times \vec{B} = -\vec{n}$. Then we require that $\nabla\psi \times \vec{n} = 0$. Figure 1 illustrates the geometry of the vectors.

The zeroth-order terms in the expansion yield $\vec{E}_0 = 0$. The first-order terms give the following conditions:

$$\vec{E}_1 \cdot \vec{n} = 0 = \vec{H}_0 \cdot \vec{n} , \quad E_{1A} = -i\sqrt{i/2}\, H_{0B} , \quad E_{1B} = i\sqrt{i/2}\, H_{0Z} , \tag{6a}$$

and

$$\nabla\psi \cdot \vec{n} = \sqrt{2i} . \tag{6b}$$

The curvature terms enter at the second order as tangential components of $\nabla \times \vec{H}_0$. We may thus evaluate the electric field and

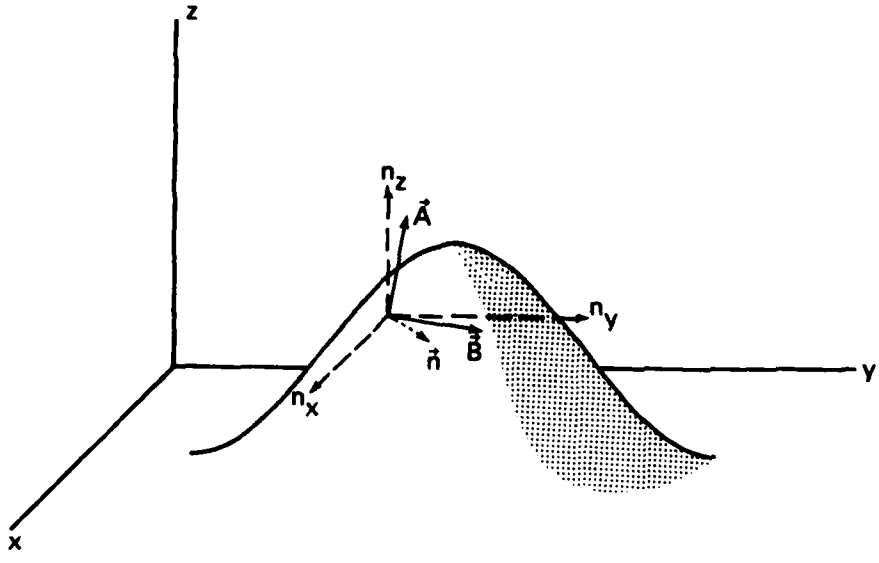

Fig. 1--Geometry for calculation of surface impedance with curvature correction

approximate it by its first three terms (the zeroth term vanishes); the resulting equation is the analog of Rytov's Eq. (12a):

$$E_A = e^{i\psi}\,\omega\mu H_{0B}\left\{-i\sqrt{i/2}\,\delta + \delta^2\left[-i\sqrt{i/2}\,\frac{H_{1B}}{H_{0B}} + \frac{1}{4}\,(\vec{A}\cdot\nabla\times\vec{B} + \vec{B}\cdot\nabla\cdot\vec{A})\right]\right\}. \tag{7}$$

Setting the curvature of the incident wave to zero and evaluating the vector products in Eq. (7) for a one-dimensional hill, we arrive at

$$\frac{E_A}{H_{0B}} = \sqrt{\mu_0/\epsilon_0}\;\frac{1}{n_g}\left[1 + \frac{\delta}{4}\,z''(y)\right], \tag{8}$$

where μ_0 and ϵ_0 are, respectively, the permeability and permittivity of free space; $\sqrt{\mu_0/\epsilon_0}$ is the impedance of free space; n_g is the index of refraction at the ground, which with the present assumptions is

$\sqrt{i\sigma/\omega\epsilon_0}$; and z"(y) is an approximation to the radius of curvature for a hill with gentle slope, where the elevation function of the hill is given as z(y).*

Equation (7) may be interpreted in terms of the focusing of the wave within the conducting medium. If the incident wave is vertically polarized, as occurs in LORAN transmission, it is appropriate to use the version of Eq. (8) that relates E_B to H_{0A}, since the sign of z" appearing in Eq. (8) uses the convention that $\vec{A}$ is the direction of the axis of the hill. The appropriate relation is found by using the transformation $\vec{A} \to \vec{B}$, $\vec{B} \to -\vec{A}$, $\vec{E} \to \vec{H}$, $\vec{H} \to -\vec{E}$. Then

$$\left|\frac{E_B}{H_{0A}}\right| = \left|\sqrt{\mu_0/\epsilon_0}\ \frac{1}{n_g}\left[1 - \frac{\delta}{4}\, z''(y)\right]\right| . \qquad (9)$$

This expression gives an easily programmable, modified impedance equal to $[1 - (\delta z''/4)]$ times the flat surface value. Our correction factor is slightly more accurate than that given by Leontovich [1944] without derivation.

Equation (9) may be interpreted physically in terms of the stretching of the electric field lines at the surface, shown schematically in Fig. 2. The $\vec{H}_0$ field is unaffected by the surface curvature. The $\vec{E}_1$ field in the ground, however, gets stretched (squeezed) as the wave front begins to diverge (converge). Energy conservation requires the electric field to change. The changes in the ratio E/H may thus be anticipated depending on whether the hill acts as a converging lens ($z'' < 1$) or a diverging lens ($z'' > 1$). The limit of validity for the series expansion is that the wave must be severely attenuated before rays cross in the ground and nonlinearities enter the problem.

*The discussion in Sec. IV uses the convention z as a function of x, the distance on a line from the transmitter to the receiver.

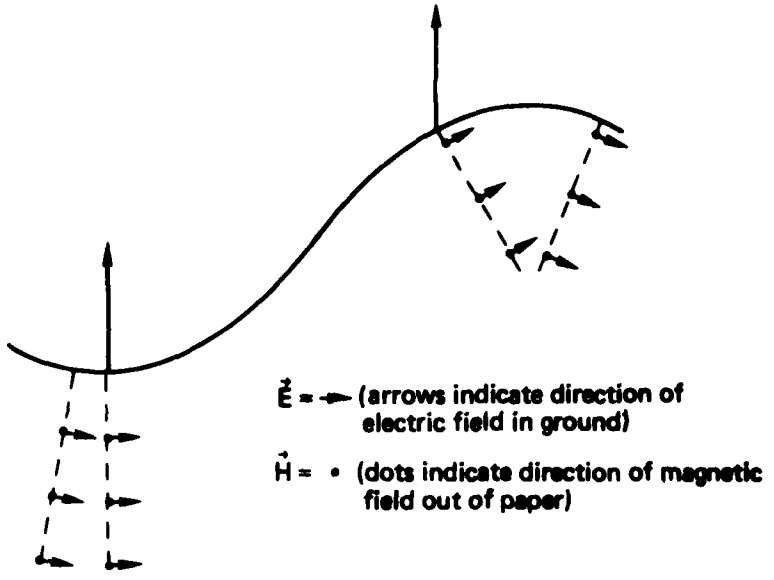

Fig. 2--Physical interpretation of surface impedance correction

III. TIME OF ARRIVAL OF THIRD-CYCLE ZERO CROSSING

For accurate LORAN timekeeping and navigation, the time of arrival of the third-cycle zero crossing of a LORAN pulse must be predicted. The Hufford equation [Hufford, 1952], used here (Sec. IV) and by others (e.g., Johler and Berry [1967]), yields the phase correction for a purely sinusoidal signal. A LORAN pulse, however, necessarily is a superposition of many frequencies, so it is appropriate to examine how accurately sole reliance on the Hufford equation at the LORAN carrier frequency predicts the propagation of a zero crossing.

A LORAN pulse F(t) can be approximated by*

$$F(t) = \sin(\omega t + \theta + \Theta)\left[\frac{t}{t_p} e^{(1-t/t_p)}\right]^2 ,$$

where $\omega = 2\pi \times 10^5$ kHz,

θ = absolute envelope to cycle difference,

$\Theta = 0$ or π,

t_p = time to peak of pulse ≈ 65 μsec.

Since such a pulse contains significant energy, distributed from 90 to 110 kHz, dispersion of the pulse must be considered in order to accurately predict the third-cycle zero crossing.

A propagating Gaussian pulse may be defined by

$$G(x, t) = \exp\left[ik_0(x - vt) - \omega_0 t\right] \exp\left[-\frac{(x - vt)^2}{2\,\Delta x^2(t)}\right] ,$$

where k_0 and ω_0 are the central wave number and frequency, respectively; v is the velocity of the pulse; and Δx is the width of the pulse. An

*Measurements by the Applied Physics Laboratory (APL) [McCarty et al., 1976] indicate that $\omega = \omega(t)$ and is not constant. That frequency drift is probably due to the particular transmitter used in APL's experiment, so is not included in our analysis.

analysis of such a pulse, familiar from discussions of quantum mechanics (e.g., Bohm [1951]), shows that the width of the pulse spreads according to

$$\Delta x(t) = \Delta x(t = 0) \sqrt{1 + \frac{\left(\frac{\partial^2 \omega}{\partial k^2}\right)^2 t^2}{[\Delta x(t = 0)]^4}} \, . \qquad (10)$$

The shape of the LORAN pulse does not significantly differ from that of a Gaussian, so our formula should fairly accurately describe the spreading of the pulse as it propagates.

If dissipation is ignored or is independent of wave number, then the center frequency is unchanged and the envelope merely spreads rather than shifting center--thus including more cycles of the carrier. Furthermore, the center of the pulse moves with the group velocity, whereas the center frequency component moves with the phase velocity. Since the two velocities are not necessarily equal, what emerges is a spreading envelope moving with a varying time (or distance) from the front of the pulse to any chosen zero crossing.

The time of arrival of the third-cycle zero crossing will be the sum of the time of arrival of the front of the pulse (when the signal exceeds the threshold of detection) plus the time for three cycles of the carrier frequency to pass. That sum does not necessarily determine the time of crossing of the third-cycle zero generated by the transmitting antenna. Since cycles are being added to the pulse, and the zeros traverse the pulse, the received third-cycle zero need not follow the front of the pulse by the same time interval as was originally generated--indeed, the received third-cycle zero could be different from the original tagged point. Figure 3 illustrates the relationship between the times of arrival of the third-cycle zero crossing t_3 and the front of the pulse t_f.

METHOD OF ANALYSIS

To analyze the above zero-crossing ambiguities, we must know the phase and group velocities as well as the spreading factor for the

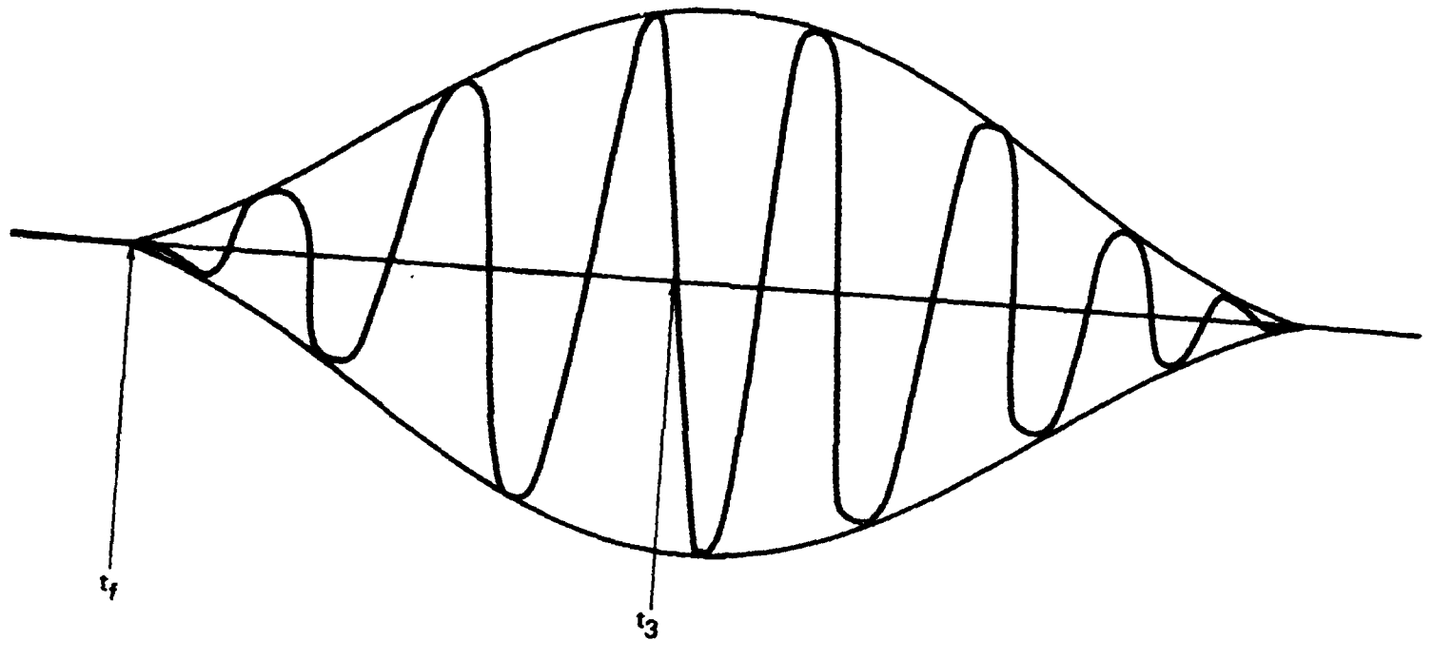

$$t_3 = \text{time of arrival} = \frac{\text{distance propagated}}{\text{velocity of envelope}} + \text{time from front to third-cycle zero crossing}$$

$$t_f = \frac{\text{distance propagated}}{\text{velocity of envelope}}$$

Fig. 3--Arrival times associated with LORAN pulse

pulse. All are, in general, obtainable from the dispersion relation for a wave. Unfortunately, the Hufford equation is not a dispersion relation since it does not give ω as an algebraic function of k. Therefore, we must numerically generate a dispersion relation by computing the phase of the signal from the Hufford equation.

The wave number k of a wave is defined locally as the gradient of the phase

$$k \equiv \frac{\partial \psi}{\partial x} ,$$

where the field Φ is equal to $|\Phi|e^{i\psi}$. The Hufford equation yields W, which is defined by $\Phi = 2W\Phi_0$, and may be considered the attenuation function of the field Φ. The free space solution is Φ_0. Thus if $W = |W|e^{i\phi}$, then

$$k(x) = \frac{\partial \phi}{\partial x} + \frac{\omega}{c} ,$$

where c is the speed of light in a vacuum.

We may evaluate the function k(x) at 90, 95, 100, 105, and 110 kHz and fit it to a second-degree polynomial at several different distances to obtain local dispersion relations of the form

$$\omega = C_1 + C_2 k + C_3 k^2 ,$$

where C_1, C_2, and C_3 are polynomial coefficients. The group velocity V_g is then

$$\left.\frac{\partial \omega}{\partial k}\right|_{100\ kHz} = 2C_3 k + C_2 ,$$

the phase velocity V_p is

$$\left.\frac{\omega}{k}\right|_{100\ kHz} = \frac{C_1}{k} + C_2 + C_3 k ,$$

and $\partial^2\omega/\partial k^2 = 2C_3$, which is needed to determine the spreading factor. Tables 1 and 2 list the resulting quantities for two different ground conductivities at various distances: the spreading factor in units of $\Delta x/\Delta x_0 - 1$ and the computed values of $V_g - V_p$.

The quantities in Table 1 show that pulse spreading is not significant over the propagation distances considered. This conclusion differs from that of Johler and Walters [1959], whose calculation showed more pulse spreading. The difference arises because we consider here an actual LORAN pulse, whereas they considered an exponentially damped cosine signal of only about one cycle in duration. Larger spread is prevented by the greater length of a LORAN pulse, as shown by the $(\Delta x_0)^4$ term appearing in Eq. (10). It is then accurate to picture the pulse as an envelope propagating along with zero crossings of the carrier signal receding (since $V_g > V_p$) from the front of the pulse.

The speed with which the phase recedes varies with distance propagated. We can estimate the distance x_0 at which phase identity difficulties are introduced into the problem by

$$\int_0^{x_0} \frac{dx}{c} (V_g - V_p) = \frac{\lambda}{2} .$$

For a ground conductivity of 0.001 mho/m, this equation yields a distance of 1500 to 2000 km. For σ = 0.01 mho/m, however, numerical results show the distance to be about ten times as far.

This argument is strongly suggestive but not numerically precise for the lower conductivity case, because such concepts as phase and group velocity are approximate in nature except when applied to pulses of infinitely narrow spectral width. The dispersion relation we used was found numerically by deriving values of k from the spatially attenuated spherical waves whose propagation is described by the Hufford equation. Since the waves from which we construct our LORAN pulse are attenuated (through W), they have a spread in k space. That spread introduces some uncertainty into the coefficients of our quadratic dispersion relation. The uncertainty in turn causes a spread in the

Table 1

SPREAD FACTORS AND PROPAGATION VELOCITIES
FOR GROUND CONDUCTIVITY OF 0.01 mho/m
AT SEVERAL DISTANCES

Distance Propagated r_0 (km)	Spreading Factor $(\Delta x/\Delta x_0 - 1)$	$V_g - V_p$ (m/sec)
76	1.7×10^{-12}	4,779.3
276	0.9×10^{-10}	8,940.9
476	5×10^{-10}	11,656.6
676	1.5×10^{-9}	13,924.8
876	3×10^{-9}	16,356.6
1,076	6×10^{-9}	17,759.5
2,076	4×10^{-8}	25,155.6
3,076	1.4×10^{-7}	31,137.9

NOTE: The group velocity is V_g and the phase velocity is V_p.

Table 2

SPREAD FACTORS AND PROPAGATION VELOCITIES
FOR GROUND CONDUCTIVITY OF 0.001 mho/m
AT SEVERAL DISTANCES

Distance Propagated r_0 (km)	Spreading Factor $(\Delta x/\Delta x_0 - 1)$	$V_g - V_p$ (m/sec)
76	2.5×10^{-9}	185,513.6
276	1×10^{-7}	315,607.6
476	3.4×10^{-7}	382,771.5
676	2.5×10^{-7}	389,607.4
876	1.5×10^{-12}	330,002.1
1,076	4.5×10^{-7}	249,938.0
2,076	2×10^{-7}	17,844.2
3,076	6×10^{-8}	2,897.4

NOTE: The group velocity is V_g and the phase velocity is V_p.

computed group speed. The precision to which we are attempting to calculate these quantities exceeds the precision of the underlying concepts--phase and group velocity.

Unfortunately, the spread in group velocity for lower conductivity cases can, at some distances, produce uncertainties of the order of the difference in the phase and group velocities. Then the only precise method of establishing the zero crossing times is to transform the LORAN pulse in the time domain to obtain the spectral density, multiply by the transfer function W, and finally invert the transform back to the time domain. The last step is known to be too complex for analytical solution. However, the first two steps of the procedure produce enough useful information to be worthwhile--e.g., how the frequency band in which most of the energy in the pulse is carried changes with distance traveled.

Figures 4 through 6 illustrate how energy partition among spectral components changes as the pulse propagates. Figure 4 gives the spectral distribution at the transmitter (derived in Appendix B). Since 99 percent of the energy lies between 90 and 110 kHz, the next two figures show, for ground conductivities of 0.01 and 0.001 mho/m, how the energy balance of the pulse changes between 76 and 3076 km, respectively. The attenuation is only slightly nonsymmetrical about 100 kHz, causing a negligible shift toward lower frequency.

CONCLUSIONS

Based on numerical computation of group effects on a LORAN pulse, we conclude

- A low-conductivity path will cause a significant drift of the third zero crossing within the pulse. At a propagation distance of about 1500 to 2000 km, cycle ambiguity can enter.
- The energy remains well centered at 100 kHz.

Except for distant receivers, therefore, the time of arrival of the third zero crossing is given accurately by the prediction of the

Hufford equation at 100 kHz. "Distant" depends on ground properties, but distances up to about 1500 km appear to present little difficulty, except for very unusual ground--e.g., Greenland ice.

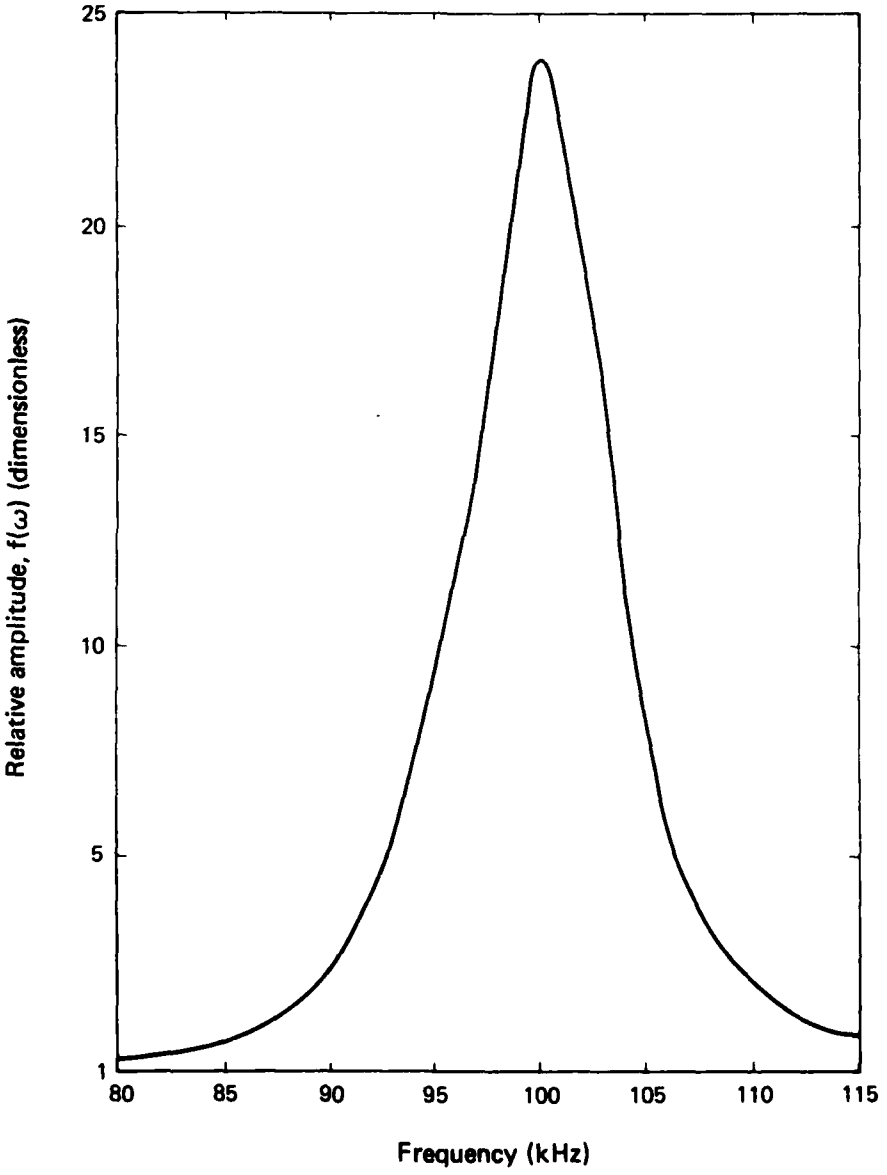

Fig. 4--Spectral distribution of transmitted pulse

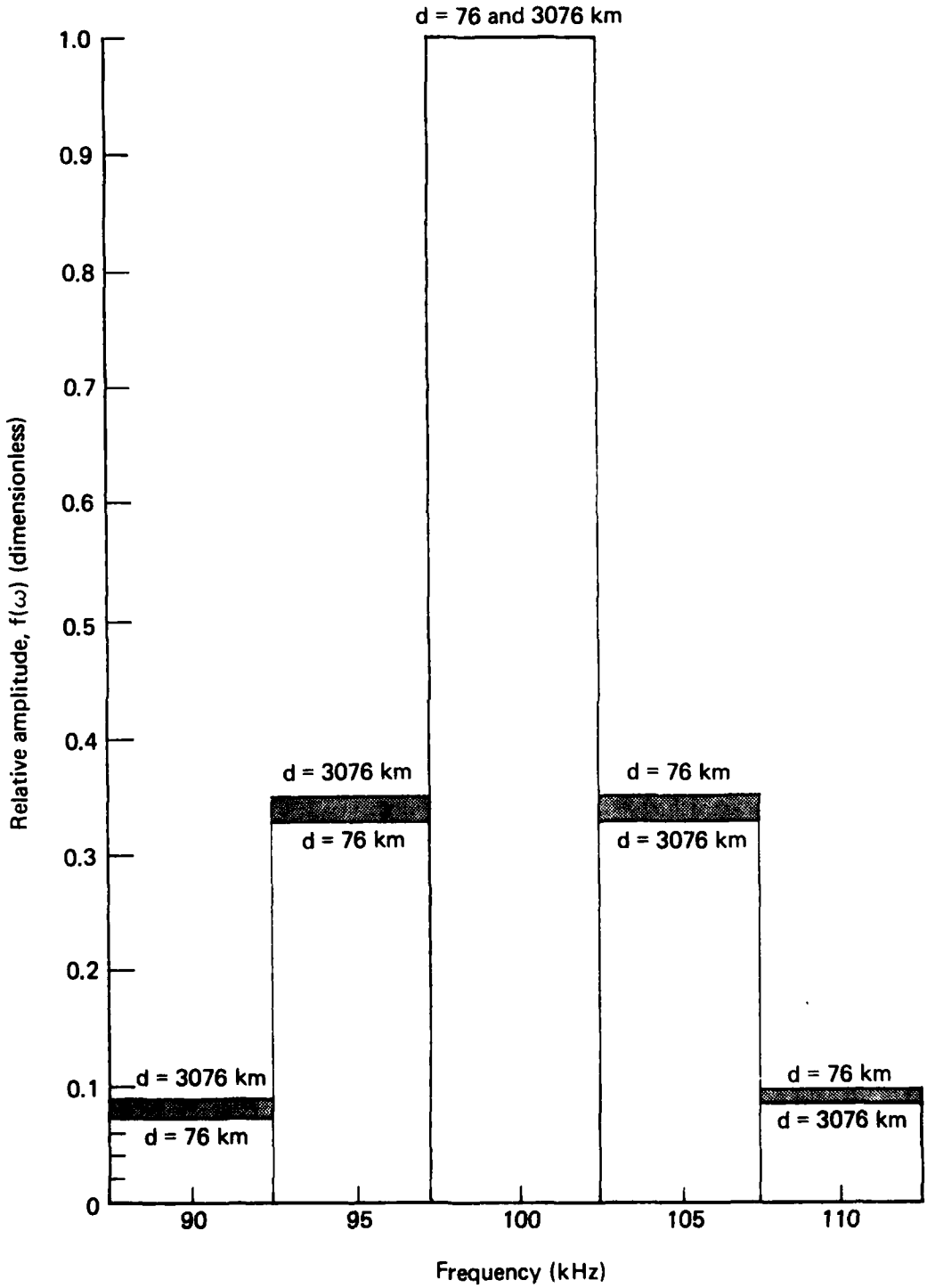

Note: This figure is normalized to 1.0 at 100 kHz for both distances. Higher frequencies are attenuated with greater distance. The gray areas show the relative change as the pulse propagates.

Fig. 5--Amplitude of transfer function of LORAN pulse at 76 and 3076 km for ground conductivity 0.01 mho/m

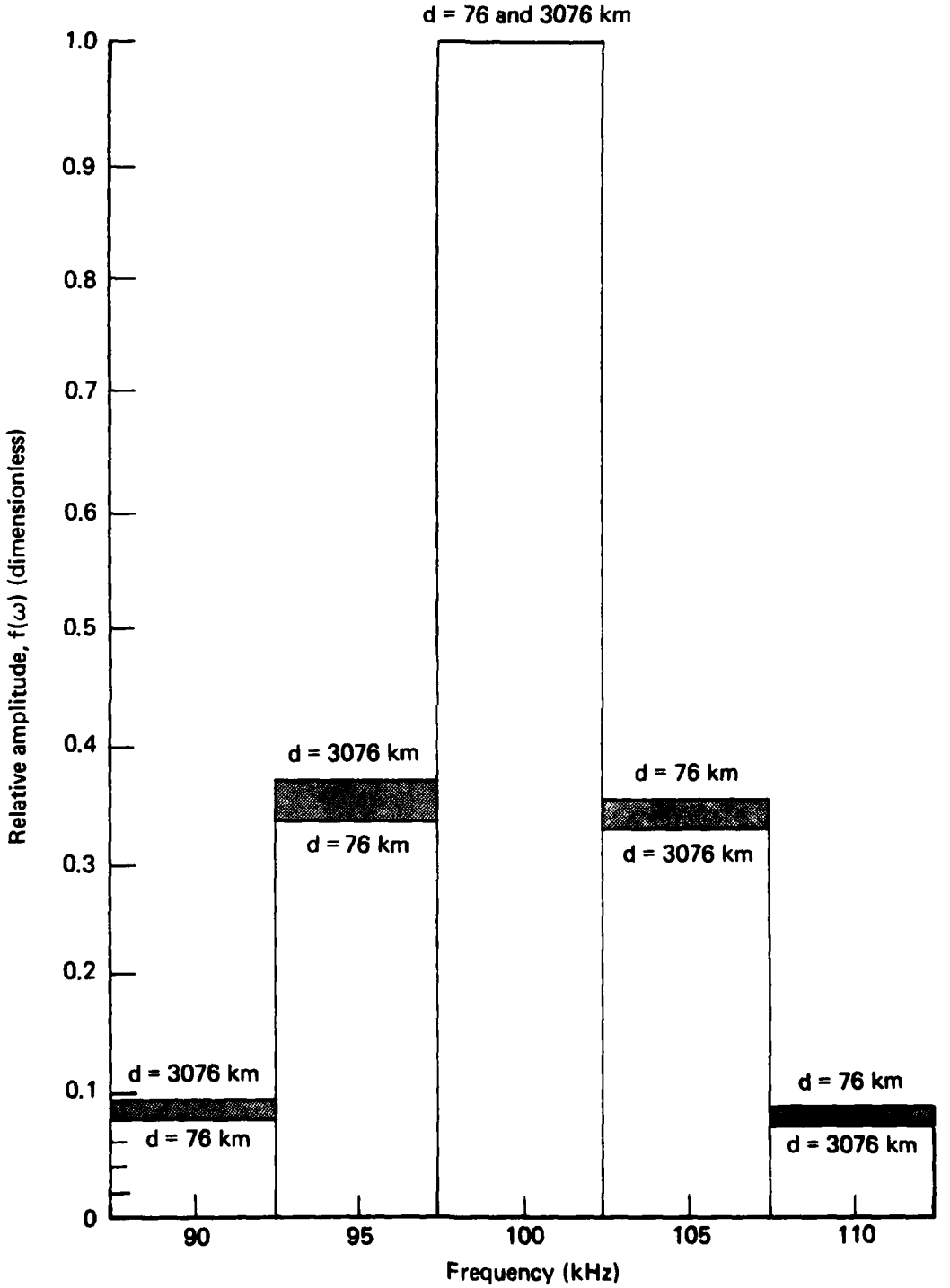

Note: This figure is normalized to 1.0 at 100 kHz for both distances. Higher frequencies are attenuated with greater distance. The gray areas show the relative change as the pulse propagates. This figure shows greater attenuation than Fig. 5.

Fig. 6--Amplitude of transfer function of LORAN pulse at 76 and 3076 km for ground conductivity 0.001 mho/m

IV. NUMERICAL STUDIES OF SURFACE PHASE PROPAGATION

Here we discuss the results of the PSR computer program for calculating the ground-wave attenuation function W--which describes how the ground wave signal differs from free space propagation--according to

$$\Phi = 2W \frac{e^{ikr}}{r} \text{ (const)} = 2W\Phi_0 \ , \tag{11}$$

where, as in Sec. III, Φ is the field in the presence of the ground and Φ_0 is the free space solution.

A previous PSR report [Field and Allen, 1978] showed that W for propagation over gentle but arbitrarily variable terrain is approximated by Hufford's Eq. (11). For convenience, we repeat that equation here:

$$W(x_0) = 1 - e^{-i\pi/4} \left(\frac{k}{2\pi}\right)^{1/2} \int_0^{x_0} dx \left[\frac{x_0}{x(x - x_0)}\right]^{1/2}$$

$$\times W(x) \left(\frac{1}{n_g} + \frac{\partial r_2}{\partial n}\right) e^{ik(r_1+r_2-r_0)} \ , \tag{12}$$

where x_0 = the distance from the transmitter to the receiver projected on a flat underlying surface,

k = the free-space wave number ω/c,

n = the unit vector normal to the ground,

n_g = the complex index of refraction, $(\kappa + i\sigma/w\varepsilon_0)^{1/2}$,

r_0 = the straight-line distance between the transmitter and the receiver,

r_1 = the straight-line distance between the transmitter and the integration point Q,

r_2 = the straight-line distance from Q to the receiver.

Figure 7a illustrates the geometry of r_0, r_1, and r_2.

a) Hill on flat earth

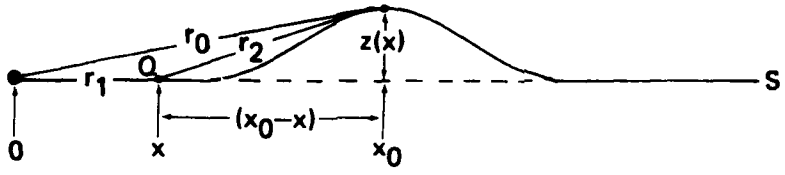

z(x) is elevation measured from surface S

b) Hill on smooth, round earth

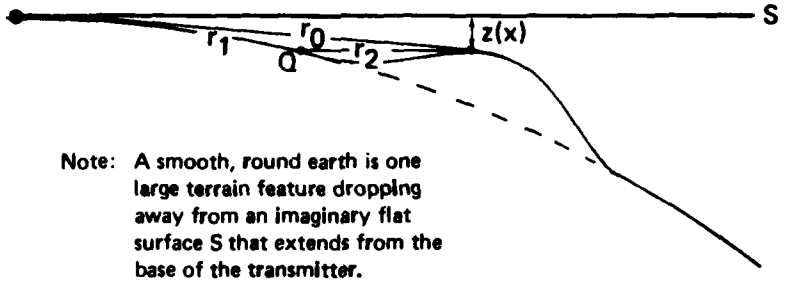

Note: A smooth, round earth is one large terrain feature dropping away from an imaginary flat surface S that extends from the base of the transmitter.

Fig. 7--Geometrical relationships among various distances in integral equations (12) and (13)

Detailed numerical analysis in Field and Allen demonstrated that Eq. (12) gives results nearly matching the well-known residue series for a smooth, round earth. In addition, that report quantitatively examined the validity criteria for Eq. (12) and derived a more exact integral equation. The basis of the PSR ground-wave computer code, Eq. (B-28) of Field and Allen is written

$$W(x_0) = 1 - e^{-i\pi/4}\left(\frac{k}{2\pi}\right)^{1/2}\int_0^{x_0} dx\,\sqrt{1+z'^2(x)}\left[\frac{r_0^2}{r_1 r_2(r_1+r_2)}\right]^{1/2}$$

$$\times\, W(x)\, e^{ik(r_1+r_2-r_0)}\left[\frac{1}{n_g}+\left(1+\frac{i}{kr_2}\right)\frac{\partial r_2}{\partial n}\right]. \qquad (13)$$

The improvements over the Hufford analysis considered here are the z" impedance correction term from Sec. II and the following differences between Eqs. (12) and (13): the extra $(i/kr_2)(\partial r_2/\partial n)$ term in Eq. (13); the $z'^2(x)$ term in Eq. (13), which represents an arc-length correction over undulating ground, z' being the derivative of the ground elevation measured with respect to a flat surface; and, finally more precise use of the distances r_0, r_1, and r_2 instead of their projections onto a flat underlying surface. The following discussion presents numerical solutions to Eq. (13) for generic terrain characteristics and shows how inclusion of the above corrections changes the calculated results.

SMOOTH EARTH

The simplest generic terrain is smooth--that is, without local elevations or depressions in an otherwise flat or spherical ground surface. For completeness and to illustrate basic properties of phase delay, we first examine propagation over a smooth surface. For a smooth, flat surface, $\partial r_2/\partial n$, z', and z" are zero--as are, therefore, all correction terms. To show how the phase delay of 100 kHz waves depends on ground conductivity in a flat earth, Fig. 8, calculated from Eq. (B-28) of Field and Allen, displays the amplitude and phase of W for conductivities of 0.01 and 0.001 mho/m. The $\sigma = 0.001$ case gives a noticeably stronger effect.

Figure 9, also calculated from Eq. (B-28), illustrates the same dependence for a round earth with no correction for $(i/kr_2)(\partial r_2/\partial n)$, z', or z". These three functions are identically zero for a flat earth, but not for a smooth, round earth--which can be thought of as a single large terrain feature, as shown in Fig. 7b above. The associated corrections are, however, too small to show significantly on a graph for a smooth, round earth with $\sigma = 0.01$ mho/m.

Figure 10 illustrates the difference between the phase of W for a smooth, flat earth and that for a smooth, round earth with all of the above corrections. Near the transmitter the difference is negligible, because of the local flatness of a round earth. When the earth's curvature causes the ground to depart by an amount of the

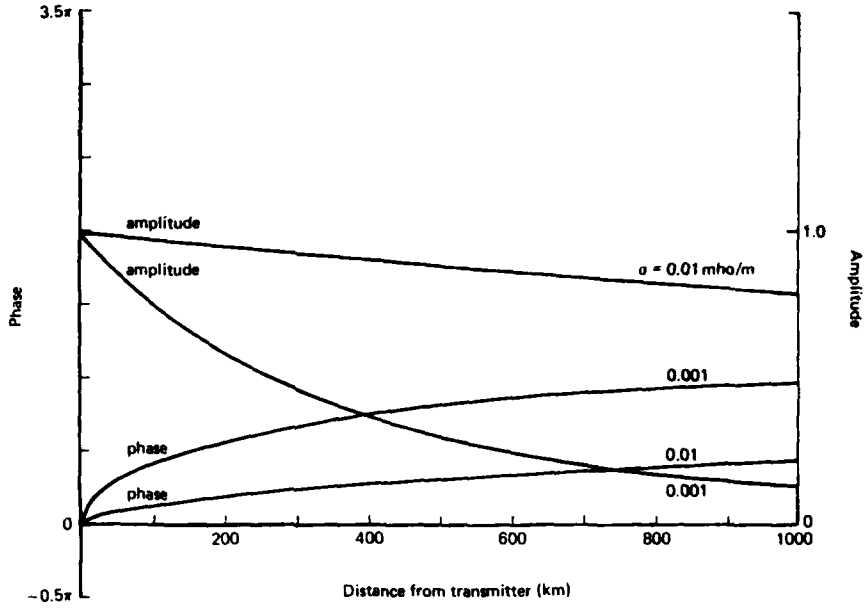

Fig. 8--Amplitude and phase of W for smooth, flat earth of conductivities 0.01 and 0.001 mho/m

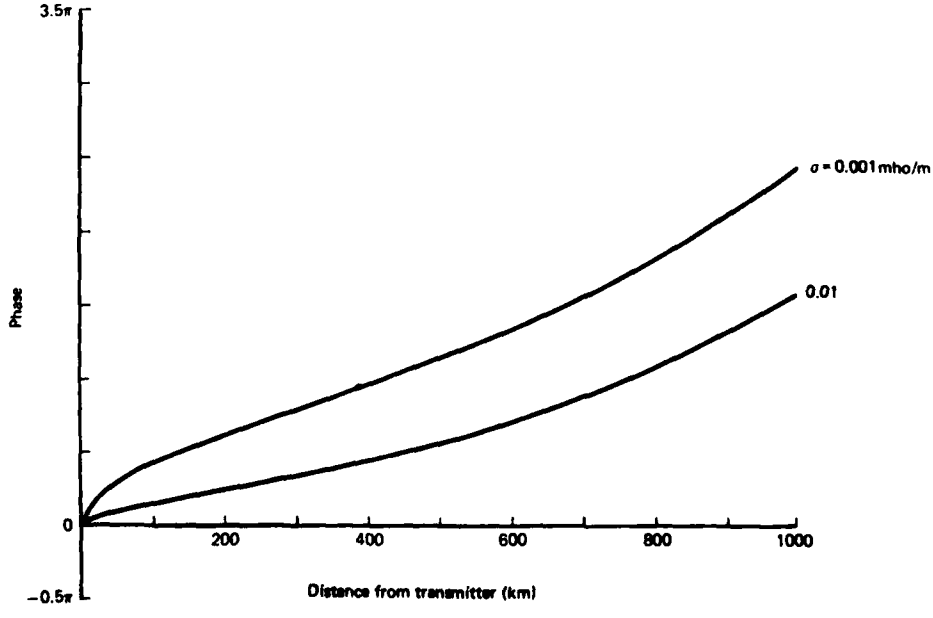

Fig. 9--Phase of W for smooth, round earth of conductivities 0.01 and 0.001 mho/m with no correction for $(i/kr_2)(\partial r_2/\partial n)$

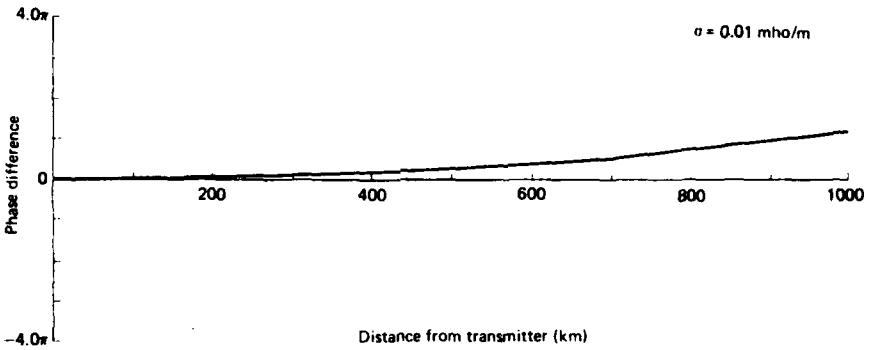

Fig. 10--Phase of W for smooth, round earth minus phase of W for smooth, flat earth

order of a wavelength from an imaginary flat surface extending from the base of the transmitter, we expect that roundness to have a significant effect. For a 100 kHz signal on the round earth, such an effect occurs at ~190 km. The ground and the imaginary surface deviate by a few percent of a wavelength at ~35 km. Thus flat and round earth results should vary little within 35 km of the transmitter and show a dramatic difference beyond ~190 km.

TERRAIN ON FLAT EARTH

Simple Ramp Terrain

Terrain influences the solution to the integral equation (13) primarily through the $\partial r_2/\partial n$ term, and secondarily through the correction terms associated with Eq. (13). Therefore, types of terrain

possessing simple forms of $\partial r_2/\partial n$ provide useful test cases from which we can build an understanding of solutions to Eq. (13). A foil against which to compare our numerical results for simple terrain is what we hereafter call the "first-order solution"--which is valid when terrain is sufficiently gentle, integration paths sufficiently short, and conductivity sufficiently high that W may be considered nearly constant and thus can be factored out of the integral on the right side of Eq. (13). The integral equation can then be solved analytically.

By virtue of the role of $\partial r_2/\partial n$ in Eq. (13), the effects of the terrain features are most readily understood in terms of the signs and magnitude of the first and second derivatives of the ground elevation. To elucidate the important effects of ground shape on W, we first consider terrain features that are a sequence of flat ramps, plotting the difference between the phases of W for various pairs of surfaces--each pair comprising a particular smooth surface and the same surface with a terrain feature. We hereafter refer to that quantity as "phase difference."

Figure 11 plots phase difference due to various rises of constant slope (ramps), each beginning 50 km from the transmitter. The steeper slopes exhibit greater phase differences at the foot of the ramp as well as greater structure in certain regions along the ramp. For moderately steep slopes, that property may be explained in terms of the first-order solution, which has monotonic behavior--slope entering merely as a multiplicative factor. For much steeper slopes, W changes too rapidly for the first-order solution to accurately describe the problem; higher order terms become significant, adding structure to the ultimate solution. Near the foot of the ramp--the point at which the second derivative of the ground elevation is significant--the phase difference is strong.

The calculations for Fig. 11 ignore the $(i/kr_2)(\partial r_2/\partial n)$ term. Its importance is illustrated for a ramp of slope 0.3 in Fig. 12, which plots the phase difference with and without the term. For slopes of 0.02 and 0.1, its effect is not noticeable on a plot of this scale. Its effect is strongest near slope changes and weakest far from a hill. The key to understanding the action of $\partial r_2/\partial n$ is to interpret it as representing the angle between the ground at an

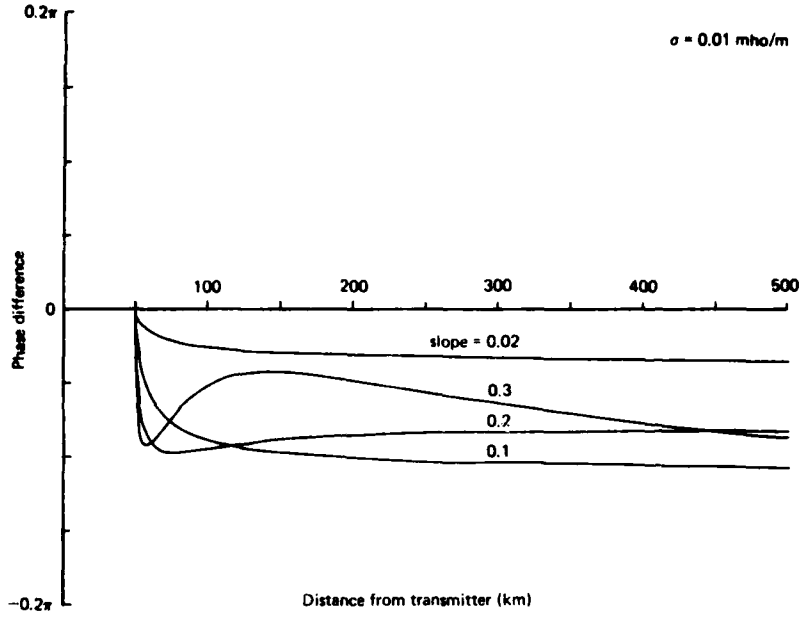

Fig. 11--Phase differences for several constant slopes beginning at 50 km, with no correction for $(i/kr_2)(\partial r_2/\partial n)$

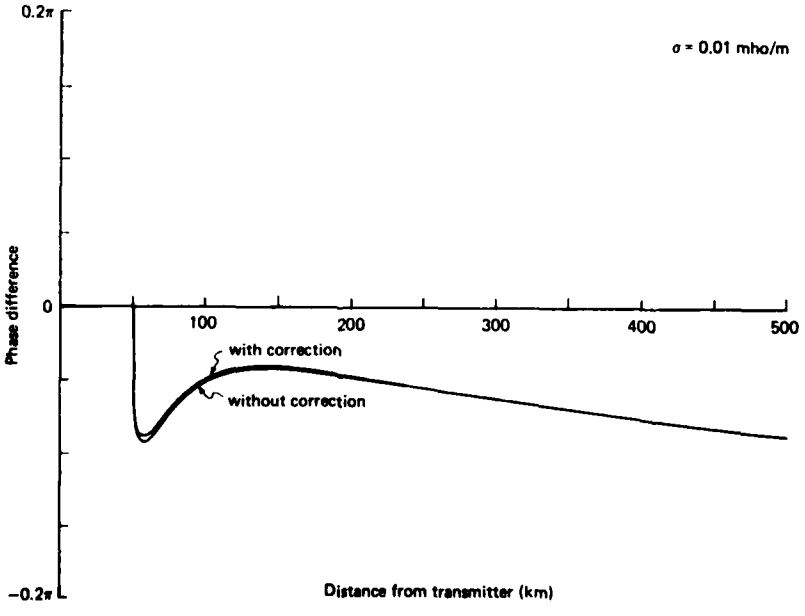

Note: The plotting points for this graph are every 2 km--a grid too coarse to show the 85 m peak difference that occurs in the first 0.1 km of the ramp and is due to inclusion of $(i/kr_2)(\partial r_2/\partial n)$.

Fig. 12--Phase difference for ramp of slope 0.3 beginning at 50 km, with and without correction for $(i/kr_2)(\partial r_2/\partial n)$

integration point and a straight line to the receiver. When the integration point and receiver are on the same flat segment, then $\partial r_2/\partial n$ is zero. On flat ground beyond a region of changing ground slope, therefore, $\partial r_2/\partial n$ is zero for integration points everywhere but on the rippled region. This is an insignificant part of the path except for receivers on or near the terrain feature. The $(i/kr_2)(\partial r_2/\partial n)$ term introduces small-scale structure near regions of strong slope change. For example, numerical calculation shows that at the foot of a 0.1 upward slope, a phase difference equivalent to 85 m appears in the first 0.1 km, which would be missed either by ignoring this term or by calculating intervals too wide to focus on the region of large second derivative. The $(i/kr_2)(\partial r_2/\partial n)$ term is included in all subsequent figures unless otherwise specified.

The stronger effect on phase of a downward-sloping ramp relative to that of a ramp of equal and opposite slope, shown in Figs. 13 and 14, cannot be explained by the first-order solution since, at that order, the phase difference is proportional to the slope of the ramp. The stronger effect is due to the magnitude of W working together with $\partial r_2/\partial n$ in the integral to produce the actual solution. Figure 15 displays the amplitude of W associated with plus and minus 0.3 slope ramps that begin 50 km from the transmitter. It shows the source of the phase difference structure exhibited in Fig. 11 for 0.3 slope. The plot of the amplitude of W for the downward-sloping ramp also exhibits the monotonic phase difference structure evident in Fig. 13 for -0.3 slope.

The arc-length correction for a 0.1 slope ramp is about 1 m in apparent propagation distance, and is thus too small to show clearly on the graphs.* On more complex terrain, the arc length may have greater effect. Its influence on phase is less than that of stretching the propagation path out flat and including the extra distance traveled, since the phase of W is a nonlinear function of distance obtained by taking the arc-tangent of the ratio of Im(W) and Re(W).

---

*The plots of phase difference scales of 0.2π can resolve phase differences of about 0.002 rad. Since 477 times the phase difference in radians gives the distance difference in meters, one meter would appear to merely thicken lines on the plot.

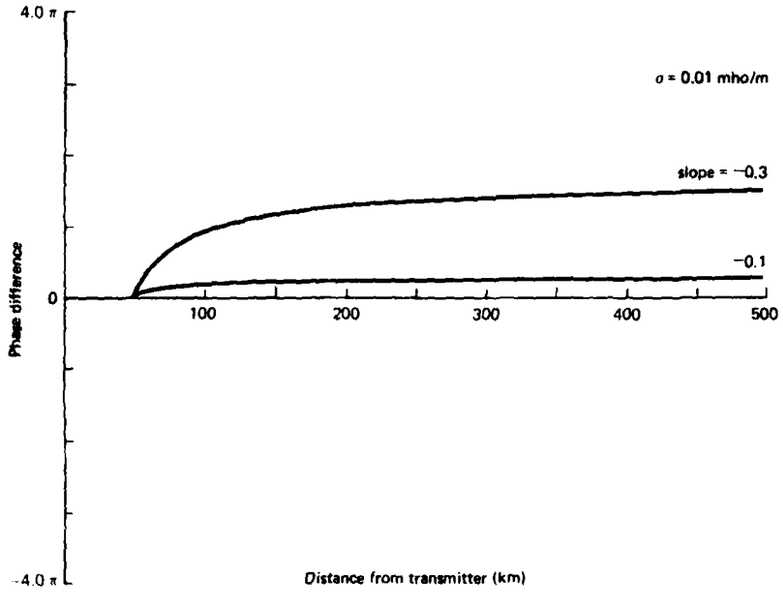

Fig. 13--Phase difference for ramps of slopes -0.1 and -0.3, both beginning at 50 km

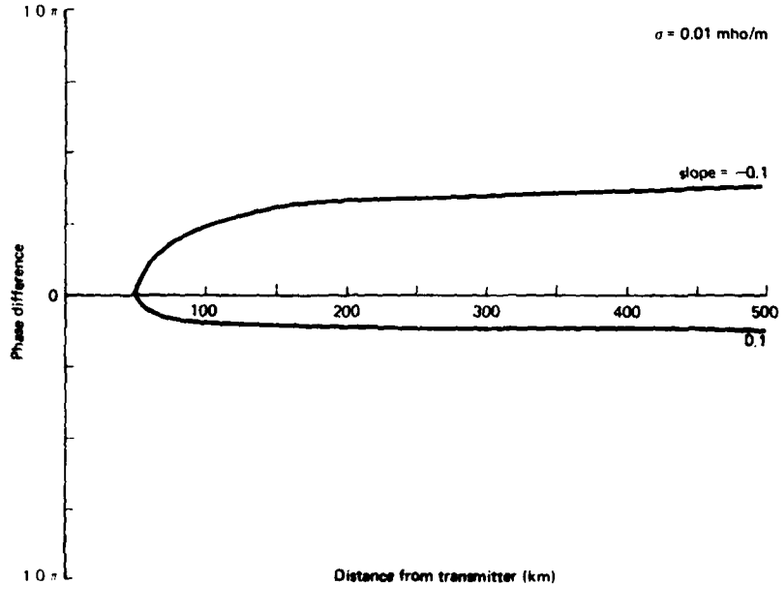

Fig. 14--Phase difference for ramps of slopes -0.1 and 0.1, both beginning at 50 km

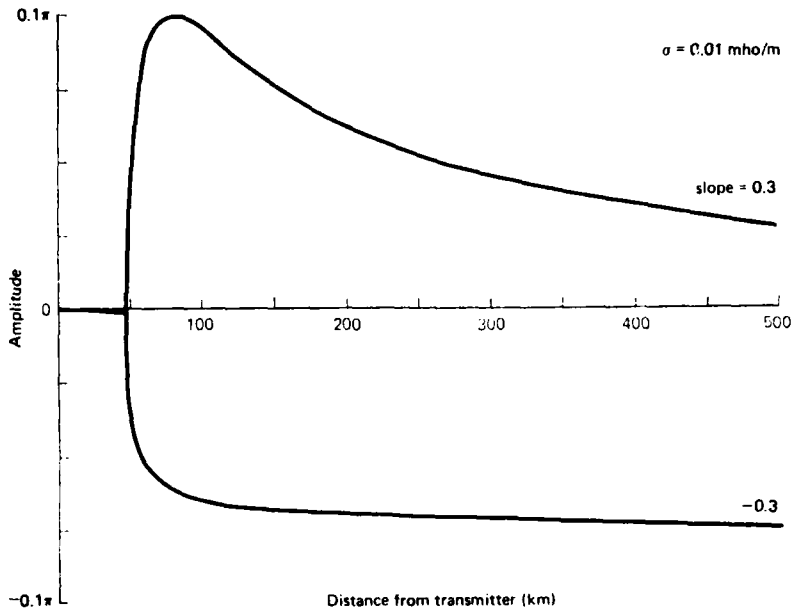

Fig. 15--Amplitude of W for ramps of slopes 0.3 and -0.3

We next consider two examples showing what happens when the slope of the ground changes abruptly. Our calculations hereafter include the arc-length correction. Figure 16 plots the phase difference associated with a ramp of slope 0.1 beginning at 50 km and changing to a 0.2 slope at 100 km. The slope of the phase difference does not change sign at the junction of the two slopes. Between 50 and 100 km, the difference matches the behavior of the 0.1 ramp found previously in Fig. 11. After 100 km, the phase difference resembles that found for the 0.2 slope in Fig. 11, but its structure is somewhat more pronounced.

The behavior of the second case is strikingly different. Figure 17 plots the phase difference associated with, again, a 0.1 ramp beginning at 50 km but changing to a 0.05 slope at 100 km. The second slope is positive and still represents an upward ramp, but

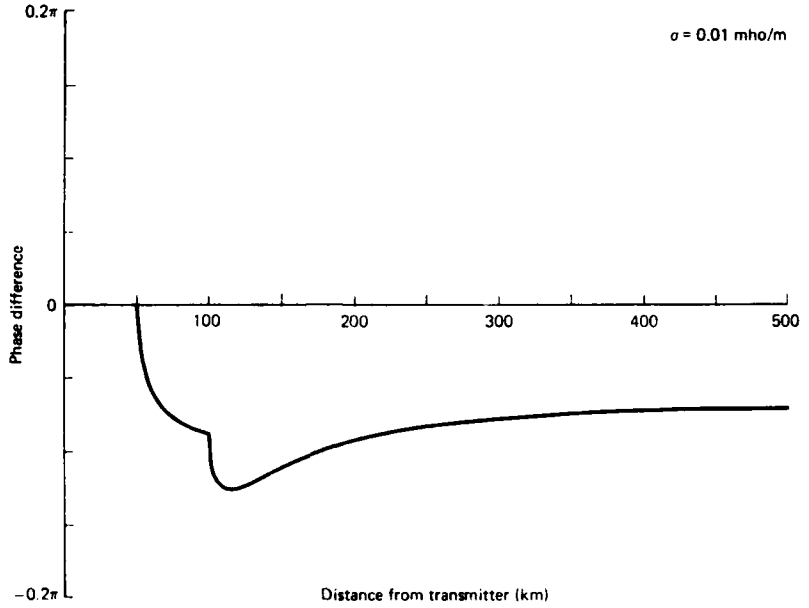

Fig. 16--Phase difference for ramp beginning at 50 km that changes slope from 0.1 to 0.2 at 100 km

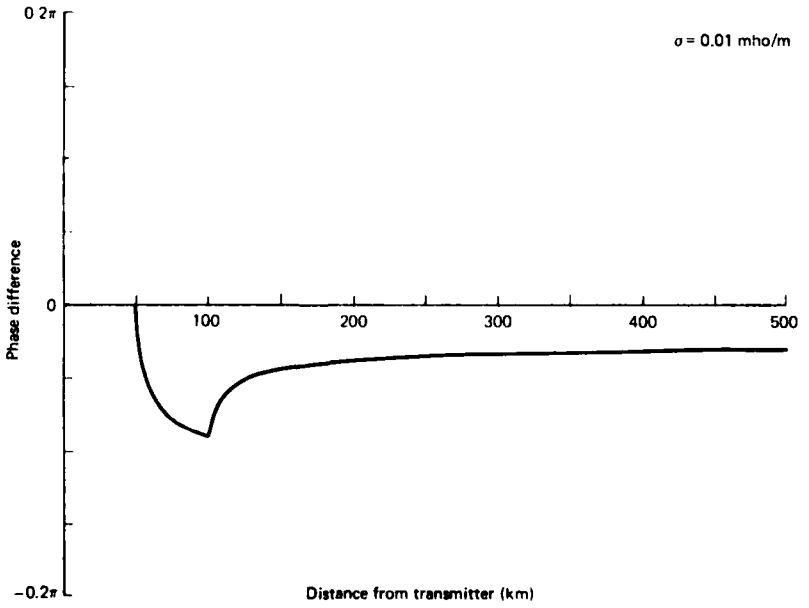

Fig. 17--Phase difference for ramp beginning at 50 km that changes slope from 0.1 to 0.05 at 100 km

not so steep as the immediately preceding 0.1 slope. Indeed, the derivative of the phase difference plot *changes sign* at the junction of the two slopes. Whereas the phase difference plot behaves in the established pattern up to 100 km, the difference associated with the 0.05 slope looks not like that of an upward ramp, but like that of a downward ramp--which it is *relative to the preceding slope*. The integral equation thus exhibits a "memory" of the ground terrain, so that the *change* in slope is a governing feature of how phase differences arise.

Referring back to Eq. (13), we see that the presence of $(1/r_2)^{1/2}$ in the integrand tends to make the slope immediately preceding the receiver most important, whereas slopes farther from the receiver contribute weakly. That sensitivity to slope change can be regarded then as sensitivity to the sign of the second derivative of the ground elevation. Thus we see a consistency in the extra structure of the phase difference for the 0.2 slope part of Fig. 16 and the inverted behavior of the 0.05 slope part of Fig. 17.

Finally, considering a one-dimensional pyramid having equal ascending and descending slopes, Fig. 18 plots the characteristic phase difference pattern for a symmetrical hill--i.e., a phase decrease (over the rising side) followed by a sharp increase (near the peak on the down side) followed by a long tail. Similar patterns have been found by others (e.g., Johler and Berry [1967]) for different symmetrical one-dimensional hills. The existence of the long tail is significant for navigation, since it indicates that a hill not only causes a local effect, but that large phase differences (perhaps many tens of meters, depending on the size of the hill) persist many hill lengths beyond the hill itself. The tail occurs because the second-derivative effect just discussed prevents the effects of the ascending and descending sides of the hill from cancelling.

Continuous-Slope Terrain

To illustrate that we have focused on the important criteria determining the effect of hill shape on phase difference patterns, we now consider some hills that have everywhere a continuously changing

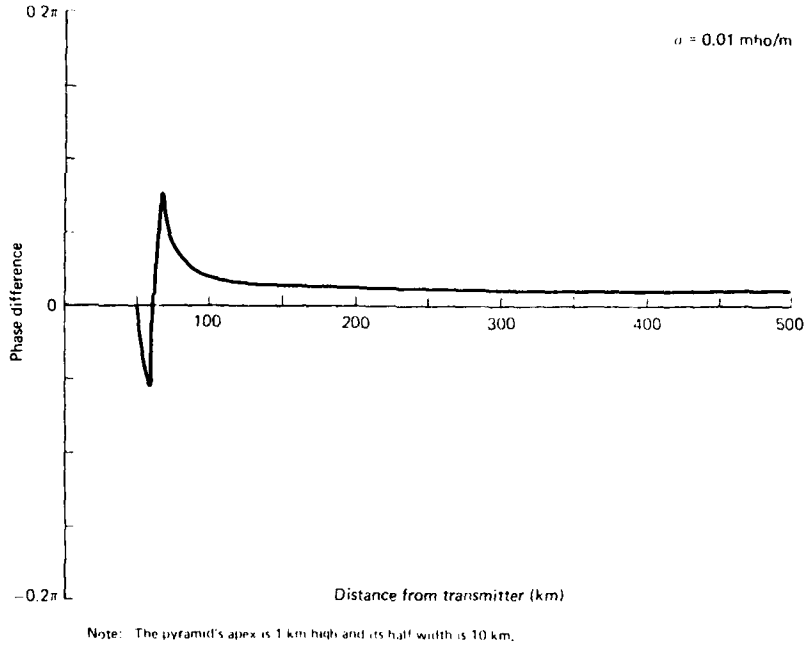

Fig. 18--Phase difference for pyramid beginning at 50 km with faces of slopes 0.1 and -0.1 (characteristic signature of symmetrical hill)

slope. We use a $1 \times 10 \sin^2(x)$ elevation function that joins smoothly with the flat ground.* The second derivative changes sign on each side of a given hill. Figure 19 shows the results of including the $(i/kr_2)(\partial r_2/\partial n)$, arc-length, and z'' impedance corrections for a $\sin^2$ hill of roughly the same proportions as the pyramid in Fig. 18. Apart from somewhat less smooth transitions at certain places, the pyramid behaves much the same as the more complicated $\sin^2$ hill.

Figure 20 directly contrasts the effect of the same two hills on phase. It is notable that merely matching height and width of the two hills yields a close match in the traces of the phase differences.

*We describe hills by giving the height times the half-width in kilometers, unless otherwise specified. We abbreviate the height function of a hill $z(x) = H \sin^2(x - x_0/L)$ as $H \times L \sin^2$. Thus a "$1 \times 10 \sin^2$" hill has a peak 1 km high, a half-width of 10 km, and a $\sin^2$ profile.

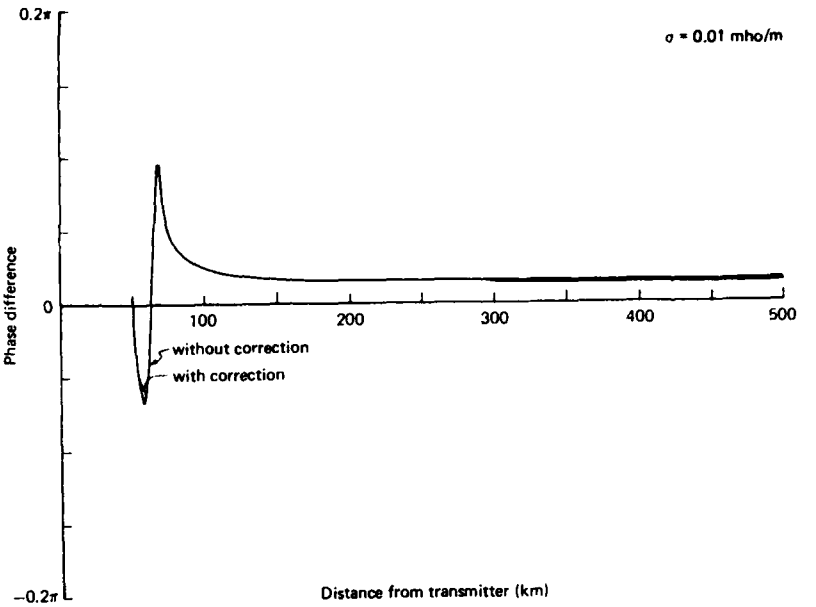

Fig. 19--Phase difference for 1 × 10 $\sin^2$ hill beginning at 50 km, with and without correction for $(i/kr_2)(\partial r_2/\partial n)$

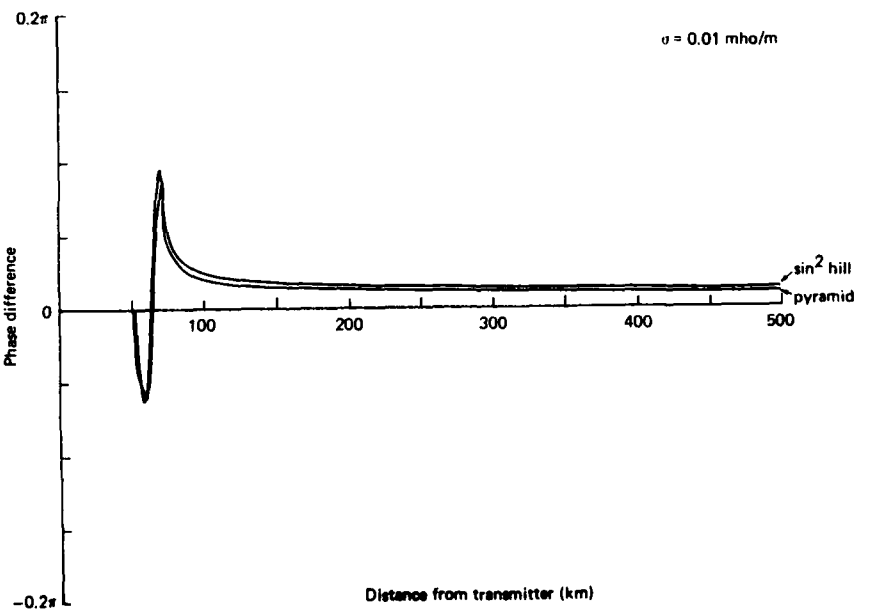

Fig. 20--Phase difference plot comparing 1 × 10 pyramid with 1 × 10 $\sin^2$ hill, both beginning at 50 km

Figure 21 illustrates how the phase difference changes over the hill when the conductivity diminishes by a factor of 10 to 0.001 mho/m. Although $1/n_g$ is much larger than before, $\partial r_2/\partial n$ is still the dominant term near the hill, so the only observable difference is in the tail and at the negative phase peak.

TERRAIN ON ROUND EARTH

Hills

Effect of Shape of Hill. Having explored the properties of hills alone, we couple the hills with round-earth propagation. Figure 22 shows three different $\sin^2$ hills 50 km from the transmitter on a round earth. The effect of the arc-length correction on the $1 \times 10 \sin^2$ hill is about 2 m in apparent propagation distance, and thus too small to show clearly on the graphs.

The z" impedance correction is negligible even for a $1 \times 3 \sin^2$ hill. We may safely ignore this factor because the impedance correction will be of consequence only when the radius of a hill becomes comparable to the skin depth (tens of meters); moreover, no reliable topographical data of such precision are available.

Effect of Distance to Hill. Now we explore the effect of hill distance from the transmitter, considering, first, hills very close to the transmitter, within the distance where earth curvature effects should be negligible; second, those at the horizon; and third, those clearly over the horizon. A hill is considered on the horizon when the line of sight from the transmitter tangent to the earth touches the top of the hill. At 110 km, a hill 1 km high sees the transmitter as being just on the horizon.

Figure 23 illustrates the subtle evolution of the signature of a symmetrical hill with increasing distance from a transmitter on a round earth. Most noticeably, the tail is larger when the distance to the transmitter is smaller. The same effect would appear on flat ground to a similar degree. For closer hills, the initial phase decrease is shallower and the peak leading into the tail is higher. This behavior is due primarily to the $(1/r_1 r_2)^{1/2}$ term in the integrand of Eq. (13), which acts as a distance weighting factor and

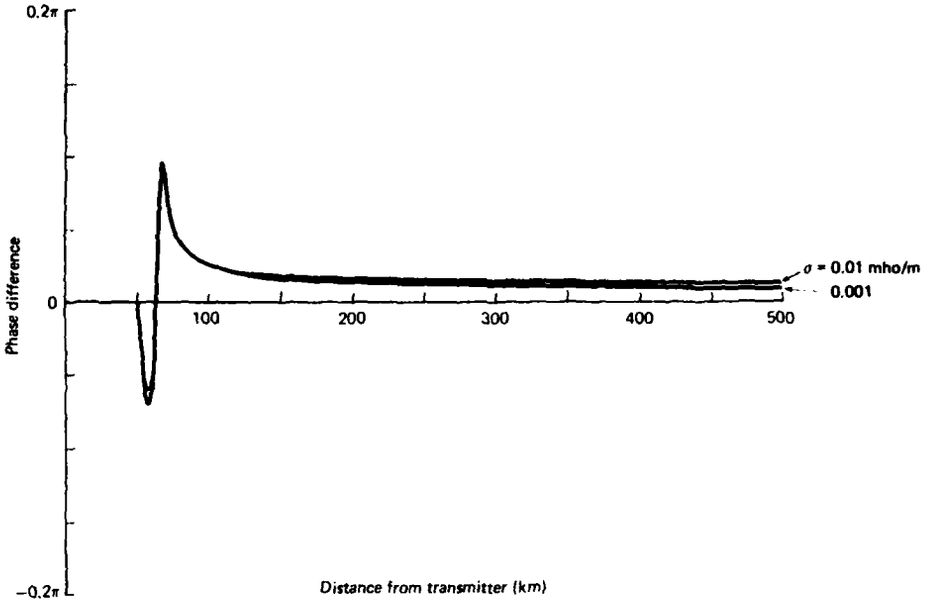

Fig. 21--Phase difference for 1 × 10 $\sin^2$ hill beginning at 50 km, with conductivities 0.01 and 0.001 mho/m

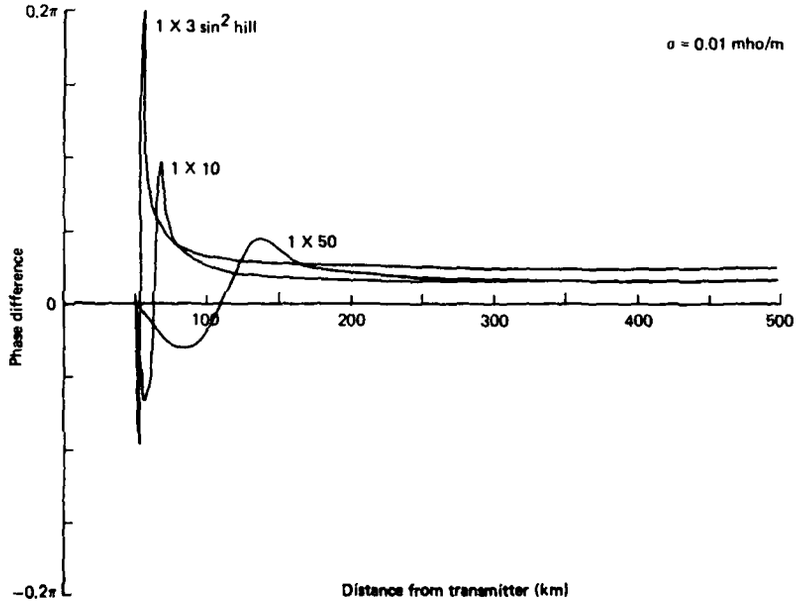

Fig. 22--Phase differences for three different $\sin^2$ hills beginning at 50 km

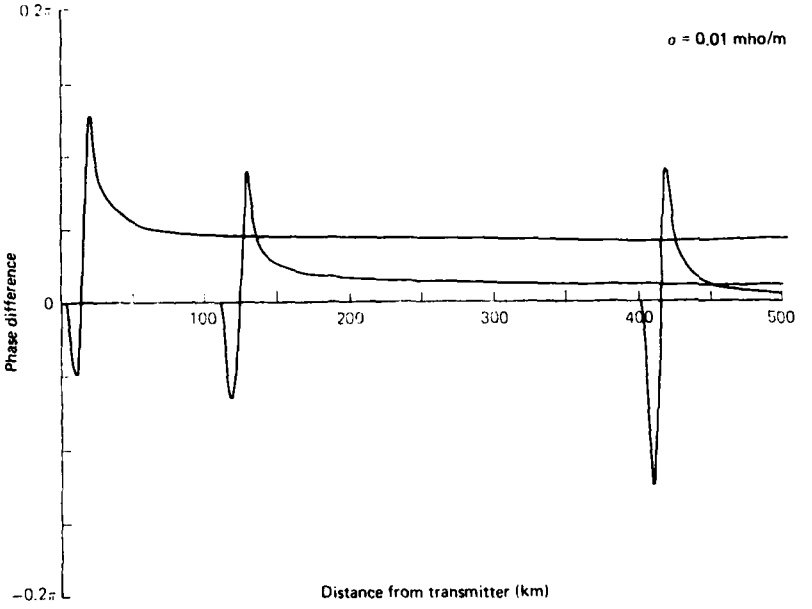

Fig. 23--Phase differences for 1 × 10 $\sin^2$ hills beginning at 5, 110, and 400 km

causes hills near the transmitter to have a stronger tail effect than those farther away.

We do not show the analogous plot for the same hills on a flat earth because it is nearly identical to Fig. 23. There is a small difference in the behavior of hills on round and flat earth because, on round earth, the slope of a face of a hill, relative to horizontal at the transmitter, depends on the slope's distance from the transmitter, as is illustrated in Fig. 24.

Proximity to the horizon seems to have no particular effect, because the receiver is on the ground. That lack of effect may be readily understood in terms of a division of the wave field into space waves and surface waves. Norton [1937] divided the field into a part that drives the ground currents and one that does not, and found that the first part drops off with height above the surface. That part is

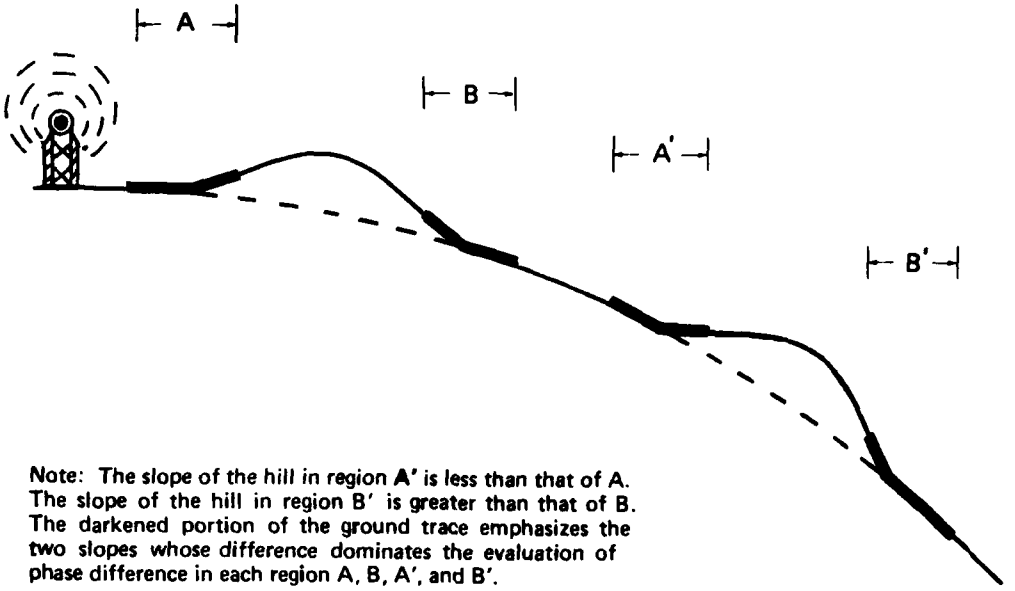

Note: The slope of the hill in region A' is less than that of A. The slope of the hill in region B' is greater than that of B. The darkened portion of the ground trace emphasizes the two slopes whose difference dominates the evaluation of phase difference in each region A, B, A', and B'.

Fig. 24--Geometry of hills near and far from transmitter

the surface wave. The other part decreases to zero at the surface and increases with height. The horizon has no effect because the surface wave component so strongly dominates the ground wave at small heights that loss of the direct wave component upon passing the horizon is unimportant.

Valleys

We next consider the effect on phase of a valley that is on the propagation path. Figure 25 compares the effect of a $1 \times 10 \sin^2$ hill with that of its $-\sin^2$ complement--i.e., valley. Although the general shapes of the phase difference plots are reflections about zero, *both* hill and valley have a positive tail. For a moderately sloped valley, such as that in Fig. 25, the incomplete mirroring of the phase difference of a hill by that of its complementary valley can be explained

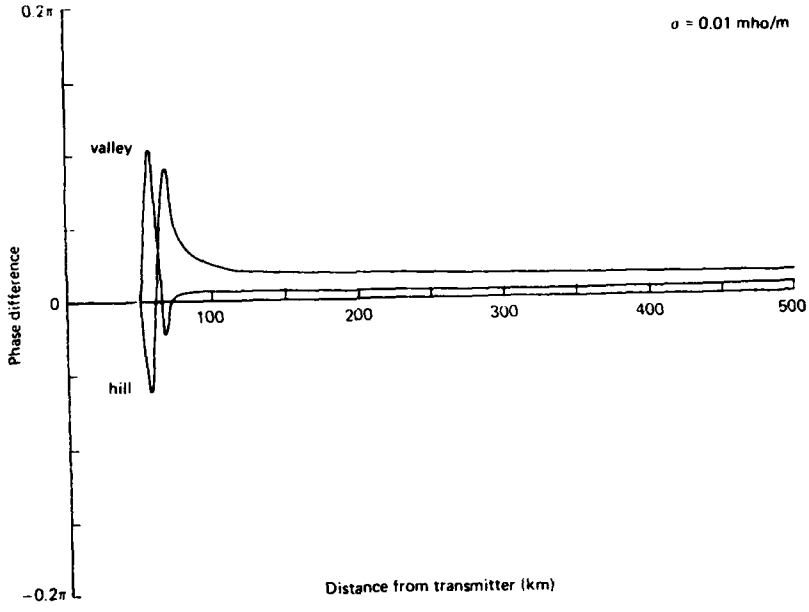

Fig. 25--Phase difference plot comparing $1 \times 10 \sin^2$ hill and valley, both beginning at 50 km

in terms of our qualitative slope and second-derivative arguments. The ground elevation function of a $\sin^2$ hill has two regions of positive second derivative and only one of negative second derivative; the valley, however, has two regions of negative second derivative and only one of positive second derivative. As discussed earlier, moderate negative second derivatives more strongly influence the phase difference than equal positive second derivatives. Such lack of symmetry in the effects of a moderate valley and the corresponding moderate hill accounts for the qualitative discrepancy in phase difference.

Slightly and steeply sloped valleys have different effects. For example, a weak $1 \times 50 \sin^2$ valley produces a phase difference that corresponds qualitatively to the predictions of a first-order

calculation and has a negative tail, as shown in Fig. 26. At the opposite extreme, we consider a hill and valley given by a 7.5×25 $\sin^2$ ground elevation function, shown in Fig. 27. These features correspond to Mt. Everest and a valley of the same size. The steep slope, long faces, and attendant large second derivatives combine to give phase differences somewhat distorted from the pattern we have found thus far. This last case also stretches the limit of applicability of the integral equation because the approximation of a Hertz potential with a single component normal to the earth is not very accurate over large portions of the integration path [Field and Allen, 1978].

Hill and Valley Combinations

Next we consider combinations of a hill and a valley. Figures 28 through 31 give the characteristic signatures of a hill followed immediately by a valley, a valley followed by a hill, and the same combinations with a smooth region the size of the hill separating the two. Rather than any tendency for each to cancel the other's effects, the plots indicate that the valley and hill keep the integrity of their signature when isolated, merely beginning on the tail of the preceding terrain feature. Notably, the major effect of a hill/valley combination is not merely the extra distance traveled by the wave. This is shown by computing the phase delay with and without the arc-length correction. The difference accounts for approximately 2 m in the distance determined from phase difference.

Minimum Significant Terrain Feature

Next we look for the minimum terrain feature that has a significant effect, in order to determine what data filtering is acceptable before applying a one-dimensional integration technique. A small individual terrain feature has a small effect. Because of the tendency of features to build onto the tail of the previous feature, however, long chains of small hills can result in large accumulated phase deviations, even if the hills' height and width are in the same 1:10 ratio we have been studying. Moreover, even for hills only 100 m high and

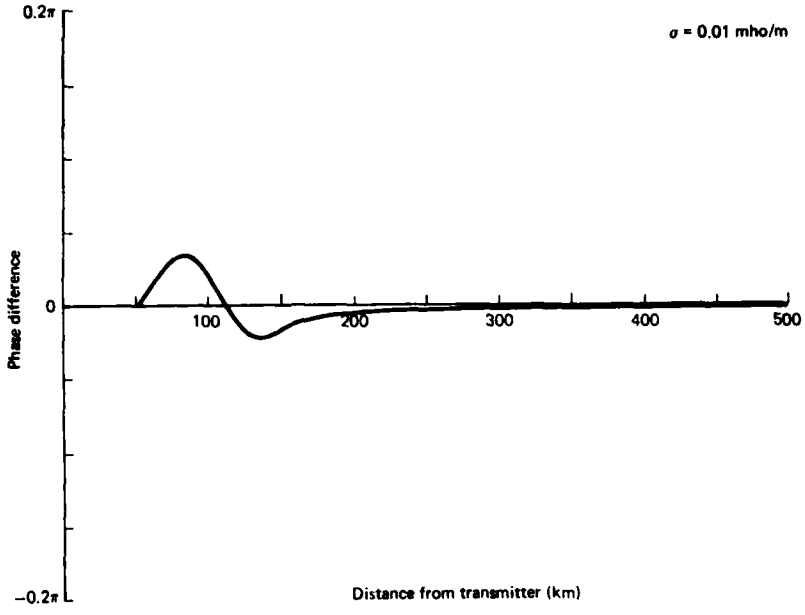

Fig. 26--Phase difference for $1 \times 50 \sin^2$ valley beginning at 50 km

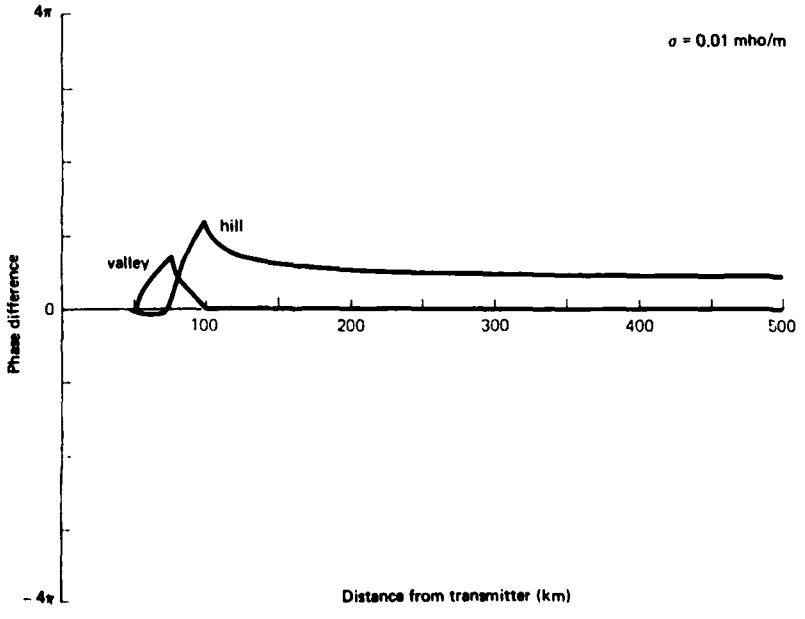

Fig. 27--Phase difference plot comparing $7.5 \times 25 \sin^2$ hill and valley, both beginning at 50 km

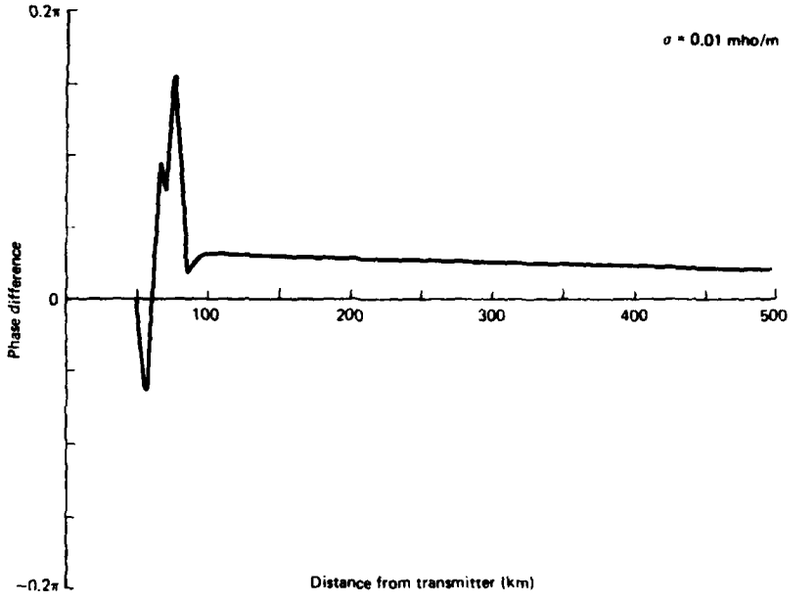

Fig. 28--Phase difference for 1 × 10 $\sin^2$ hill beginning at 50 km, followed by 1 × 10 $\sin^2$ valley beginning at 70 km

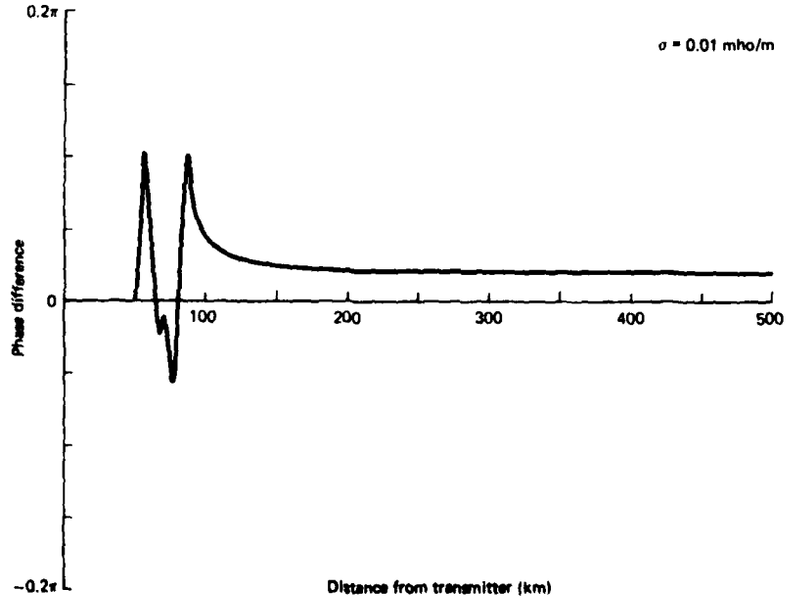

Fig. 29--Phase difference for 1 × 10 $\sin^2$ valley beginning at 50 km, followed by 1 × 10 $\sin^2$ hill beginning at 70 km

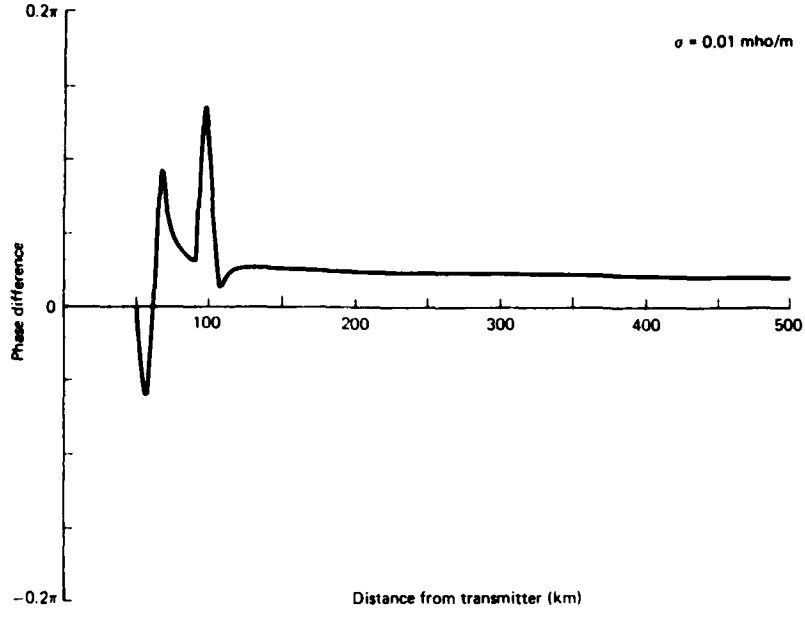

Fig. 30--Phase difference for 1 × 10 $\sin^2$ hill beginning at 50 km, followed by 1 × 10 $\sin^2$ valley beginning at 90 km

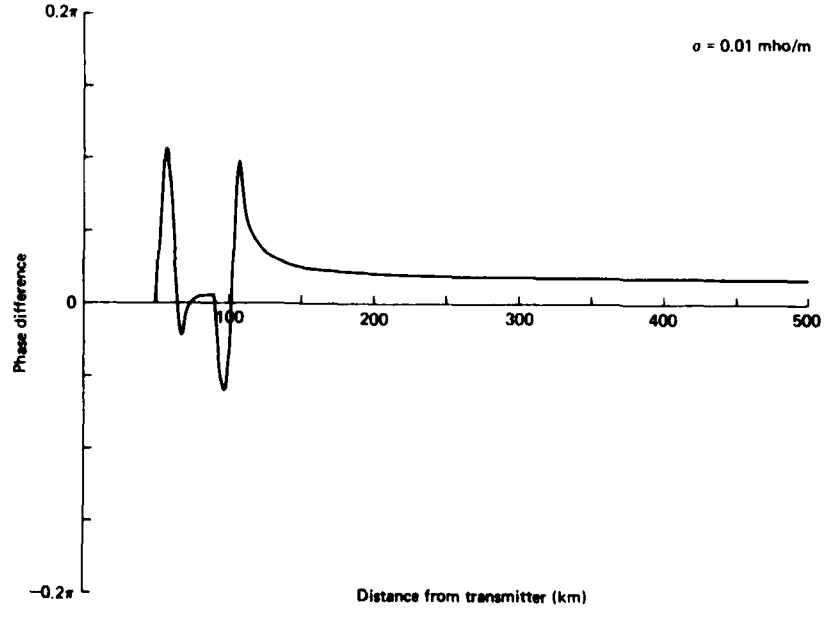

Fig. 31--Phase difference for 1 × 10 $\sin^2$ valley beginning at 50 km, followed by 1 × 10 $\sin^2$ hill beginning at 90 km

1000 m long, a sequence of 10 hills can produce a maximum phase difference equivalent to approximately 40 m. Longer sequences produce larger accumulated phase differences. Figures 32 through 34 illustrate such behavior.

The present analysis indicates that a sufficiently long chain of hills--however small the individual hills--will produce a noticeable phase shift. This result is not to be expected of real terrain, which generally has transverse and longitudinal extensions of similar dimensions. Isolated ridges are common, but not extended series of ridges. The small features thus are not realistically represented by the present one-dimensional treatment. Field and Joiner [1979] have shown that the effect of an obstacle occluding a small portion of a Fresnel zone is reduced *pro rata* from that of an obstacle filling the Fresnel zone. Extension to infinity in the transverse direction has little more effect than just filling the Fresnel zone.

More explicitly, the one-dimensional approximation (13) to the full-fledged two-dimensional equation (C.1) assumes no ground structure in the transverse direction. The phase difference for hill chains just calculated is analogous to propagation across the ridges of washboard-like terrain wide enough to fill a Fresnel zone of width

$$\sqrt{(\text{wave length}) \times (\text{receiver distance from transmitter})} \ .$$

The width of a Fresnel zone at 200 km, for example, is $\sqrt{3 \text{ km} \times 200 \text{ km}} \simeq 25$ km. A chain of hills 1 km long and 25 km wide is unlikely to extend many kilometers. One would be more likely to find terrain with many scattered hills about 1 km long and about 1 km wide. A single such hill would have roughly 1/25 the effect of a hill 1 km long and 25 km wide. Of course, the hill 25 km wide would fill the Fresnel zone and have essentially the same effect as an infinitely wide hill. More precise evaluation of the effect of obstacles small relative to the width of a Fresnel zone requires recourse to the two-dimensional integral equation (C.1).

CONCLUSIONS

We have presented numerical results for a variety of possible

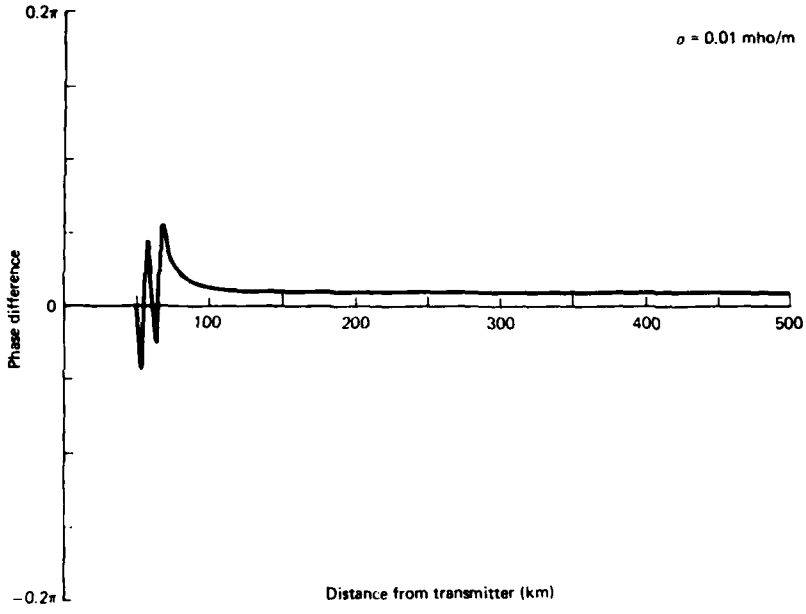

Fig. 32--Phase difference for sequence of two $0.5 \times 5 \sin^2$ hills

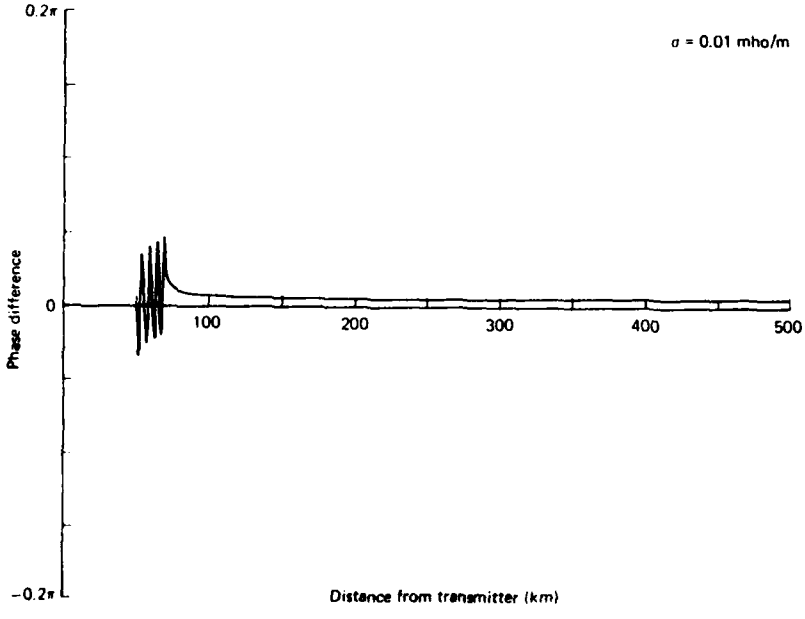

Fig. 33--Phase difference for sequence of four $0.25 \times 2.5 \sin^2$ hills

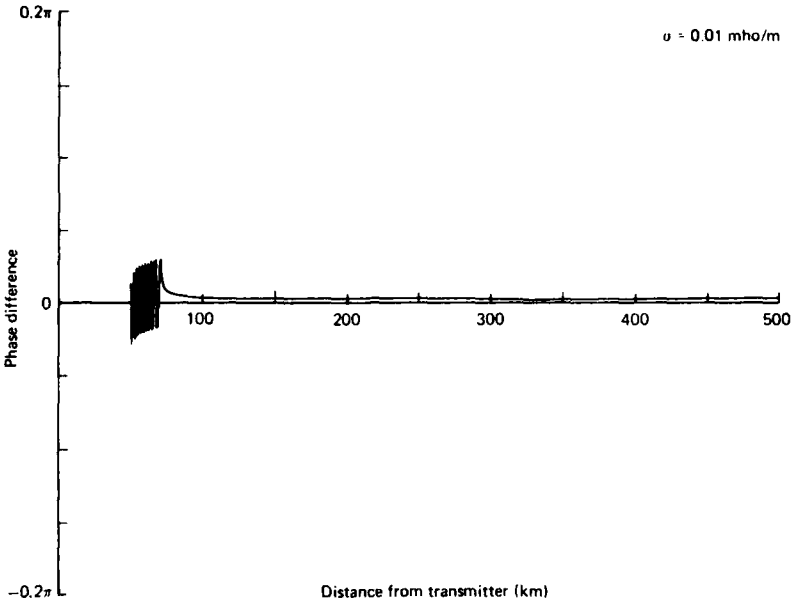

Fig. 34--Phase difference for sequence of ten $0.1 \times 1.0 \sin^2$ hills

terrain configurations with an eye toward determining which factors are significant in modifying the calculated time of arrival of phase for a 100 kHz signal. We conclude the following:

- Terrain features produce local and distant perturbations in propagation of phase relative to a smooth surface. Such effects are characteristic of the type of terrain feature encountered (e.g., hill, valley) and can be equivalent to many tens of meters of receiver-to-transmitter distance on smooth ground even for gentle terrain over distances of a few hundred kilometers.
- The significance of arc length and curvature-modified impedance corrections is small, amounting to a few meters under typical conditions. The inclusion of the $(i/kr_2)(\partial r_2/\partial n)$ term is important, especially in regions of large slope change such as at the base of a hill.

- The magnitude of the effect of a particular terrain feature is insignificantly affected by whether the underlying smooth surface is flat or round.
- Comparing Fig. 19, which illustrates a $\sin^2$ hill and a pyramid of the same length and height, with Fig. 9, which shows the effect of different ground conductivities on phase, we find that knowledge of ground conductivity is more critical than knowledge of the exact shape of a terrain feature.
- Sequences of terrain features yield phase differences roughly equivalent to those resulting from starting the phase difference patterns of subsequent bumps on the tail of preceding ground features. Since such an effect is cumulative, many small bumps will significantly alter the effective distance as determined by phase arrival. The one-dimensional integral equation (13) will overestimate the effect of such terrain, which will rarely fill the entire width of a Fresnel zone.

REFERENCES

Bohm, D., *Quantum Theory*, Prentice-Hall, Englewood Cliffs, New Jersey, 1951.

Fehlner, L. F., et al., *Summary Report on USAF Super Receiver/Navigator Development*, Johns Hopkins University, Applied Physics Laboratory, TG 1220, June 1973.

Field, E. C., and R. Allen, *Propagation of the Low-Frequency Groundwave over Nonuniform Terrain*, Rome Air Development Center, RADC-TR-78-68, March 1978, A057273.

-----, and R. G. Joiner, "An Integral-Equation Approach to Long-Wave Propagation in a Nonstratified Earth-Ionosphere Waveguide," *Radio Science*, Vol. 14, No. 6, 1979.

Hufford, G. A., "An Integral Equation Approach to the Problem of Wave Propagation over an Irregular Surface," *Quart. Appl. Math.*, Vol. 9, No. 4, 1952, pp. 391-403.

Johler, J. R., and L. A. Berry, *LORAN Phase Corrections over Inhomogeneous Irregular Terrain*, Institute for Telecommunications Sciences and Aeronomy, Boulder, Colorado, ESSA Technical Report IER 59-ITSA-56, 1967.

-----, and L. C. Walters, "Propagation of a Ground Wave Pulse around a Finitely Conducting Spherical Earth from a Damped Sinusoidal Source Current," *IRE Trans. Antennas and Propagation*, Vol. AP-7, No. 1, January 1959, pp. 1-10.

Leontovich, M. A., "Approximate Boundary Conditions for the Electromagnetic Field on the Surface of a Good Conductor," *Bull. Acad. Sci. USSR, Sec. Phys.*, Vol. 9, No. 16, 1944.

McCarty, T. A., et al., *Experimental Research on the Propagation of LORAN-C Signals*, Johns Hopkins University, Applied Physics Laboratory, APL/JHU-TG 1298, 1976.

Norton, K. A., "The Propagation of Radio Waves over the Surface of the Earth and in the Upper Atmosphere: II. The Propagation from Vertical, Horizontal, and Loop Antennas over a Plane Earth of Finite Conductivity," *Proc. IRE*, Vol. 25, No. 9, September 1937, pp. 1203-1236.

Rytov, S. M., "The Calculation of the Skin-Effect by the Method of Perturbation," *J. Expl. and Theor. Phys.*, Vol. 10, No. 2, 1940, p. 180 (in Russian); trans. R. L. Allen, Pacific-Sierra Research Corporation, Note 176, December 1977.

Senior, T.B.A., "Impedance Boundary Conditions for Imperfectly Conducting Surfaces," *Appl. Sci. Res., Sect. B*, Vol. 8, 1961, pp. 418-436.

Appendix A

DERIVATION OF CURVATURE CORRECTION TO SURFACE IMPEDANCE

Performing a detailed derivation of Eq. (8) (Sec. II, p. 5), we calculate here the impedance E/H for the case of a wave propagating at the surface of a curved conductor, with a correction for curvature. Figure 1 (p. 5) illustrates the geometry of the problem.

We proceed from the following two Maxwell equations:

$$\nabla \times \vec{E} = -\mu \frac{\partial \vec{H}}{\partial t} , \tag{A.1}$$

and

$$\nabla \times \vec{H} = \sigma \vec{E} . \tag{A.2}$$

We assume the fields to be of the following forms, respectively:

$$\vec{E} = \vec{e}\omega\mu \exp\left\{ i \left[\frac{\psi(x, y, z)}{\delta} - \omega t \right] \right\}$$

$$= (\vec{E}_0 + \delta\vec{E}_1 + \delta^2\vec{E}_2 + \cdots)e^{i(\psi/\delta - \omega t)} , \tag{A.3}$$

and

$$\vec{H} = \vec{h} \exp\left\{ i \left[\frac{\psi(x, y, z)}{\delta} - \omega t \right] \right\}$$

$$= (\vec{H}_0 + \delta\vec{H}_1 + \delta^2\vec{H}_2 + \cdots)e^{i(\psi/\delta - \omega t)} . \tag{A.4}$$

The skin depth δ is given by

$$\delta = \left(\frac{2}{\omega\sigma\mu} \right)^{\frac{1}{2}} . \tag{A.5}$$

Equation (A.1) thus becomes

$$\nabla \times \vec{E} = i\omega\mu\vec{H} \ ,$$

which may be written as independent component equations:*

$$\begin{aligned}
\nabla_x \times \vec{e} - \frac{i}{\delta}\,(e_y\psi_{,z'} - e_z\psi_{,y'}) &= ih_x \ , \\
\nabla_y \times \vec{e} - \frac{i}{\delta}\,(e_z\psi_{,x'} - e_x\psi_{,z'}) &= ih_y \ , \\
\nabla_z \times \vec{e} - \frac{i}{\delta}\,(e_x\psi_{,y'} - e_y\psi_{,x'}) &= ih_z \ .
\end{aligned} \tag{A.6}$$

Similarly rewriting Eq. (A.2) yields

$$\begin{aligned}
\nabla_x \times \vec{h} = \frac{i}{\delta}\,(h_y\psi_{,z'} - h_z\psi_{,y'}) &= \omega\sigma\mu e_x \ , \\
\nabla_y \times \vec{h} = \frac{i}{\delta}\,(h_z\psi_{,x'} - h_x\psi_{,z'}) &= \omega\sigma\mu e_y \ , \\
\nabla_z \times \vec{h} = \frac{i}{\delta}\,(h_x\psi_{,y'} - h_y\psi_{,x'}) &= \omega\sigma\mu e_z \ .
\end{aligned} \tag{A.7}$$

A prime on a differentiating subscript denotes that the coordinate is in units of skin depth, e.g., $y' = y/\delta$.

We now describe the surface locally by two unit tangent vectors, $\vec{A}$ and $\vec{B}$, and a normal $\vec{n}$ pointing into the conductor with components (n_x, n_y, n_z). The condition of normal propagation is that $\vec{\nabla}\psi$ be along $\vec{n}$ so that $\vec{\nabla}\psi \times \vec{n} = 0$. Therefore, we now write

$$\psi_{,y} = \psi_{,z}\,\frac{n_y}{n_z} \ ,$$

*For simplicity of notation, hereafter we use a comma followed by a subscript to denote partial differentiation, e.g., $\psi_{,z} \equiv \partial\psi/\partial z$.

and

$$\psi_{,x} = \psi_{,z} \frac{n_x}{n_z} .$$

From Eq. (A.5) it follows that $\sigma = 2/(\omega\mu\delta^2)$, so we may rewrite with an explicit ordering of δ the equation sets (A.6) and (A.7):

$$\delta(\nabla_x \times \vec{e}) - i\left(e_y\psi_{,z'} - e_z\psi_{,z'}\frac{n_y}{n_z}\right) = i\delta h_x , \tag{A.8a}$$

$$\delta(\nabla_y \times \vec{e}) - i\left(e_z\psi_{,z'}\frac{n_x}{n_z} - e_x\psi_{,z'}\right) = i\delta h_y , \tag{A.8b}$$

$$\delta(\nabla_z \times \vec{e}) - i\left(e_x\psi_{,z'}\frac{n_y}{n_z} - e_y\psi_{,z'}\frac{n_x}{n_z}\right) = i\delta h_z , \tag{A.8c}$$

and

$$\delta^2(\nabla_x \times \vec{h}) - i\delta\left(h_y\psi_{,z'} - h_z\psi_{,z'}\frac{n_y}{n_z}\right) = 2e_x , \tag{A.9a}$$

$$\delta^2(\nabla_y \times \vec{h}) - i\delta\left(h_z\psi_{,z'}\frac{n_x}{n_z} - h_x\psi_{,z'}\right) = 2e_y , \tag{A.9b}$$

$$\delta^2(\nabla_z \times \vec{h}) - i\delta\left(h_x\psi_{,z'}\frac{n_y}{n_z} - h_y\psi_{,z'}\frac{n_x}{n_z}\right) = 2e_z . \tag{A.9c}$$

The δ^0 terms yield

$$-i\left(E_{0y}\psi_{,z'} - E_{0z}\psi_{,z'}\frac{n_y}{n_z}\right) = 0 ,$$

$$-i\left(E_{0z}\psi_{,z'}\frac{n_x}{n_z} - E_{0x}\psi_{,z'}\right) = 0 ,$$

$$-i\left(E_{0x}\psi_{,z'}\frac{n_y}{n_z} - E_{0y}\psi_{,z'}\frac{n_x}{n_z}\right) = 0 .$$

For a hill, as shown in Fig. 1 (p. 5), $n_x = n_y = n_z$ is excluded. The last set of equations then implies

$$E_{0x} = E_{0y} = E_{0z} = 0 \ . \tag{A.10}$$

Proceeding to the terms of order δ^1 that appear in Eqs. (A.8a-c) and (A.9a-c), it is found that $\vec{n} \cdot \vec{H}_0 = 0$ and $\vec{n} \cdot \vec{E}_1 = 0$. The same terms may also be combined to obtain

$$H_{0x} = \frac{H_{0z} \frac{n_x}{n_z} \psi'^2 + \frac{n_x n_y}{n_z^2} \psi'^2 H_{0y}}{\psi'^2 \left(1 + \frac{n_y^2}{n_z^2}\right) - 2i} \ ,$$

$$H_{0x} = \frac{H_{0z} \left(-\frac{n_y}{n_z} \psi'^2\right) + H_{0y} \left[-2i + \psi'^2 \left(1 + \frac{n_x^2}{n_z^2}\right)\right]}{\frac{n_y n_x}{n_z^2} \psi'^2} \ , \tag{A.11}$$

$$H_{0x} = \frac{H_{0z} \left[-2i + \psi'^2 \left(\frac{n_x^2}{n_z^2} + \frac{n_y^2}{n_z^2}\right)\right] + H_{0y} \left(-\frac{n_y}{n_z} \psi'^2\right)}{\frac{n_x}{n_z} \psi'^2} \ ,$$

where $\psi' = \psi_{,z'}$. If we require these equations to be consistent for all values of H_{0y} and H_{0z}, then the respective coefficients of H_{0y} and H_{0z} must be equal. That equality leads to the condition

$$\frac{\psi'}{n_z} = +\sqrt{2i} \ . \tag{A.12}$$

But

$$\vec{\nabla}\psi \cdot \vec{n} = \psi_{,x} n_x + \psi_{,y} n_y + \psi_{,z} n_z$$

$$= \psi_{,z} \frac{n_x^2}{n_z} + \psi_{,z} \frac{n_y^2}{n_z} + \psi_{,z} \frac{n_z^2}{n_z}$$

$$= \frac{\psi'}{n_z} .$$

The derivative of the phase ψ in the normal direction is thus $\pm\sqrt{2i}$. Considering the refractive material to be a hill with free space above, we want the field to attenuate with decreasing z. We thus choose the + sign in Eq. (A.12).

Because of Eq. (A.12), the field resulting from terms of order δ^1 obeys

$$E_{1A} = \frac{1}{\sqrt{2i}} H_{0B} = -i\sqrt{i/2}\, H_{0B} \qquad \text{(A.13a)}$$

and

$$E_{1B} = \frac{1}{\sqrt{2i}} H_{0A} = i\sqrt{i/2}\, H_{0A} . \qquad \text{(A.13b)}$$

These two equations are obtained simply by projecting the δ^1 result onto the $\vec{A}$ and $\vec{B}$ basis vectors.

Then, taking projections onto the $\vec{A}$, $\vec{B}$ basis of the δ^2 terms and using previous results to simplify, after lengthy calculation, we obtain the following set of equations:

$$(\nabla \times \vec{E}_1)_A - i \frac{\psi'}{n_z} E_{2B} = iH_{1A} , \qquad (A.14a)$$

$$(\nabla \times \vec{E}_1)_B + i \frac{\psi'}{n_z} E_{2A} = iH_{1B} , \qquad (A.14b)$$

$$(\nabla \times \vec{E}_1)_n = iH_{1n} , \qquad (A.14c)$$

$$(\nabla \times \vec{H}_0)_A - i \frac{\psi'}{n_z} H_{1B} = 2E_{2A} , \qquad (A.14d)$$

$$(\nabla \times \vec{H}_0)_B + i \frac{\psi'}{n_z} H_{1A} = 2E_{2B} , \qquad (A.14e)$$

$$(\nabla \times \vec{H}_0)_n = 2E_{2n} . \qquad (A.14f)$$

If Eq. (A.14) is to have a self-consistent solution, then (A.14a) and (A.14e) must yield $(\nabla \times \vec{E}_1)_A = i\sqrt{i/2}\ (\nabla \times \vec{H}_0)_B$, (A.14b) and (A.14d) must yield

$$(\nabla \times \vec{E}_1)_B = \sqrt{i/2}\ (\nabla \times \vec{H}_0)_A , \qquad (A.15)$$

and (A.14d) must yield $E_{2A} = -i\sqrt{i/2}\ H_{1B} + 1/2(\nabla \times \vec{H}_0)_A$.

Recall that the electric field of our wave is

$$E_A = \delta E_{1A} + \delta^2 E_{2A} + \cdots .$$

Substituting for E_{1A} and E_{2A} from Eqs. (A.13a) and (A.15),

$$E_A = \delta(-i\sqrt{i/2}\ H_{0B}) + \delta^2[-i\sqrt{i/2}\ H_{1B} + 1/2(\nabla \times \vec{H}_0)_A + \cdots] . \qquad (A.16)$$

The H_{1B} term is associated with the curvature of the incident wave front and, for this problem, we let $H_{1B} = 0$. We evaluate $1/2(\nabla \times \vec{H}_0)_A$, assuming

$$(\nabla \times \vec{E}_1)_A = i\sqrt{i/2}\ (\nabla \times \vec{H}_0)_B \ ,$$

$$(\nabla \times \vec{E}_1)_B = -i\sqrt{i/2}\ (\nabla \times \vec{H}_0)_A \ ,$$

$$E_{1A} = -i\sqrt{i/2}\ H_{0B} \ , \quad E_{1B} = i\sqrt{i/2}\ H_{0A} \ ,$$

$$H_{Cn} = E_{1n} = 0 \ .$$

After considerable algebra, we obtain

$$(\nabla \times \vec{H}_0)_A = 1/2\ H_{0B}(\vec{A} \cdot \nabla \times \vec{B} + \vec{B} \cdot \nabla \times \vec{A}) \ . \tag{A.17}$$

We then have

$$E_A = e^{i\psi}\ \omega\mu H_{0B}\delta(-i\sqrt{i/2})\left[1 + \frac{\delta}{4}\ (\vec{A} \cdot \nabla \times \vec{B} + \vec{B} \cdot \nabla \times \vec{A})\right]. \tag{A.18}$$

For a hill with no variation in the $\vec{A}$ direction = x direction, $\nabla \times \vec{A} = 0$ and

$$\vec{A} \cdot \nabla \times \vec{B} = \vec{B}_{z,y} = \frac{\partial^2 z}{\partial y^2}\left[1 + \left(\frac{\partial z}{\partial y}\right)^2\right]^{-\frac{1}{2}}\left\{2\left(\frac{\partial z}{\partial y}\right)^2\left[1 + \left(\frac{\partial z}{\partial y}\right)^2\right]^{-1} + 1\right\}$$

$$= \frac{z''(y)}{1 + z'^2}\ (1 + 3z'^2)$$

$$\simeq z'' \tag{A.19}$$

for small z'^2. Then, for the impedance of the surface,

$$\frac{E_A}{H_{0B}} = \sqrt{\mu_0/\epsilon_0}\ \frac{1}{n_g}\left(1 + \frac{\delta}{4}\ z''\right). \tag{A.20}$$

Appendix B

CALCULATION OF LORAN SPECTRAL INTENSITY FUNCTION

To analyze group effects, we must know the intensity at all frequencies of a LORAN pulse. Here we derive the functional form of the LORAN pulse in the frequency domain plotted by Fig. 4 (Sec. III, p. 15)--which, when multiplied by W, is the basis for Figs. 5 and 6.

A single LORAN pulse has the form

$$F(t) = \left(\frac{t}{t_p}\right)^2 e^{2(1-t/t_p)} \sin(\omega_0 t + \theta) , \qquad x = 0,\ t \geq 0 . \tag{B.1}$$

We assume that each pulse effectively decays to zero before the emission of the following pulse. We further assume that propagation effects are not so severe as to ever cause pulses to overlap. Thus we may analyze only a single pulse. The spectral intensity is

$$f(\omega,\ x = 0) = \frac{1}{(2\pi)^{1/2}} \int_{-\infty}^{\infty} F(t) e^{-i\omega t}\, dt . \tag{B.2}$$

If we define step(t) = 1 for t > 0, 0 otherwise, then

$$f(\omega,\ 0) = \frac{1}{(2\pi)^{1/2}} \int_{-\infty}^{\infty} \text{step}(t) \left[\frac{t}{t_p} e^{(1-t/t_p)}\right]^2 \sin(\omega_0 t + \theta) e^{-i\omega t}\, dt$$

$$= \frac{1}{(2\pi)^{1/2}} \frac{e^2}{t_p^2} \int_{-\infty}^{\infty} \text{step}(t)\ t^2\, e^{-2t/t_p} \sin(\omega_0 t + \theta) e^{-i\omega t}\, dt$$

$$= \frac{1}{(2\pi)^{1/2}} \frac{e^2}{t_p^2} \int_{0}^{\infty} t^2 \sin(\omega_0 t + \theta) e^{-(i\omega + 2/t_p)t}\, dt . \tag{B.3}$$

Let

$$p = i\omega + \frac{2}{t_p} , \tag{B.4}$$

so

$$f(\omega, 0) = \frac{1}{(2\pi)^{1/2}} \frac{e^2}{t_p^2} \int_0^\infty t^2 \sin (\omega_0 t + \theta) e^{-pt} \, dt . \tag{B.5}$$

Then

$$f(\omega, 0) = \frac{1}{(2\omega)^{1/2}} \frac{e^2}{t_p^2} \mathcal{L}[t^2 \sin (\omega_0 t + \theta)]$$

$$= \frac{1}{(2\pi)^{1/2}} \frac{e^2}{t_p^2} \frac{d^2}{dp^2} \mathcal{L}[\sin (\omega_0 t + \theta)] . \tag{B.6}$$

Using

$$\sin (\omega_0 t + \theta) = \sin \omega_0 t \cos \theta + \cos \omega_0 t \sin \theta , \tag{B.7}$$

we obtain

$$f(\omega, 0) = \frac{1}{(2\pi)^{1/2}} \frac{e^2}{t_p^2} \frac{d^2}{dp^2} \left[\cos \theta \, \mathcal{L}(\sin \omega_0 t) + \sin \theta \, \mathcal{L}(\cos \omega_0 t) \right]$$

$$= \frac{\cos \theta}{(2\pi)^{1/2}} \frac{e^2}{t_p^2} \frac{d^2}{dp^2} \left[\omega_0 \left(p^2 + \omega_0^2 \right)^{-1} \right]$$

$$+ \frac{\sin \theta}{(2\pi)^{1/2}} \frac{e^2}{t_p^2} \frac{d^2}{dp^2} \left[p \left(p^2 + \omega_0^2 \right)^{-1} \right] . \tag{B.8}$$

Now

$$\frac{d}{dp}\left(p^2 + \omega_0^2\right)^{-1} = -\left(p^2 + \omega_0^2\right)^{-2} 2p \ , \tag{B.9}$$

$$\frac{d^2}{dp^2}\left(p^2 + \omega_0^2\right)^{-1} = 2\left(p^2 + \omega_0^2\right)^{-3} 4p^2 - 2\left(p^2 + \omega_0^2\right)^{-2}$$

$$= \frac{2}{\left(p^2 + \omega_0^2\right)^2}\left(\frac{4p^2}{p^2 + \omega_0^2} - 1\right) , \tag{B.10}$$

$$\frac{d}{dp}\, p\left(p^2 + \omega_0^2\right)^{-1} = p\,\frac{d}{dp}\left(p^2 + \omega_0^2\right)^{-1} + \left(p^2 + \omega_0^2\right)^{-1} , \tag{B.11}$$

and

$$\frac{d^2}{dp^2}\, p\left(p^2 + \omega_0^2\right)^{-1} = p\,\frac{d^2}{dp^2}\left(p^2 + \omega_0^2\right)^{-1} + \frac{2d}{dp}\left(p^2 + \omega_0^2\right)^{-1}$$

$$= \frac{2p}{\left(p^2 + \omega_0^2\right)^2}\left(\frac{4p^2}{p^2 + \omega_0^2} - 1\right) - 4p\left(p^2 + \omega_0^2\right)^{-2}$$

$$= \frac{2p}{\left(p^2 + \omega_0^2\right)^2}\left(\frac{4p^2}{p^2 + \omega_0^2} - 3\right) . \tag{B.12}$$

Therefore,

$$f(\omega, 0) = \frac{2p}{\left(p^2 + \omega_0^2\right)^2}\,\frac{1}{(2\pi)^{1/2}}\,\frac{e^2}{t_p^2}\left[\cos 0\left(\frac{4p^2}{p^2 + \omega_0^2} - 1\right) + \sin\theta\left(\frac{4p^2}{p^2 + \omega_0^2} - 3\right)\right]$$

$$= \frac{2p}{\left(p^2 + \omega_0^2\right)^3}\,\frac{1}{(2\pi)^{1/2}}\,\frac{e^2}{t_p^2}\left[\left(3p^2 - \omega_0^2\right)\cos\theta + \left(p^2 - 3\omega_0^2\right)\sin\theta\right] . \tag{B.13}$$

Let us take $\theta = 0$. Then

$$f(\omega, 0) = \frac{2p}{\left(p^2 + \omega_0^2\right)^3} \frac{1}{(2\pi)^{1/2}} \frac{e^2}{t_p^2} \left(3p^2 - \omega_0^2\right) . \qquad (B.14)$$

Using

$$p = i\omega + \frac{2}{t_p} , \qquad p^2 = -\omega^2 + \frac{i4\omega}{t_p} + \frac{4}{t_p^2} ,$$

we obtain

$$\mathrm{Re}f(\omega, 0) = n \left[\left(-3\omega^2 - \omega_0^2 + \frac{12}{t_p^2}\right) m - \left(\frac{12\omega}{t_p}\right) \ell\right] \qquad (B.15)$$

and

$$\mathrm{Im}f(\omega, 0) = n \left[\frac{12\omega}{t_p} \; m + \left(-3\omega^2 - \omega_0^2 + \frac{12}{t_p^2}\right) \ell\right] , \qquad (B.16)$$

where

$$n = \frac{2e^2/t_p^2}{(2\pi)^{1/2} \left[\left(\omega_0^2 - \omega^2 + \frac{4}{t_p^2}\right)^2 + \left(\frac{4\omega}{t_p}\right)^2\right]^3} ,$$

$$m = \frac{2}{t_p} \left[\left(\omega_0^2 - \omega^2 = \frac{4}{t_p^2}\right)^3 - 3\left(\omega_0^2 - \omega^2 + \frac{4}{t_p^2}\right)\left(\frac{4\omega}{t_p}\right)^2\right]$$

$$- \omega \left[\left(\frac{4\omega}{t_p}\right)^3 - 3\left(\omega_0^2 - \omega^2 + \frac{4}{t_p^2}\right)^2 \frac{4\omega}{t_p}\right] ,$$

and

$$\ell = \frac{2}{t_p}\left[\left(\frac{4\omega}{t_p}\right)^3 - 3\left(\omega_0^2 - \omega^2 + \frac{4}{t_p^2}\right)^2 \frac{4\omega}{t_p}\right]$$

$$+ \omega\left[\left(\omega_0^2 - \omega^2 + \frac{4}{t_p^2}\right)^3 - 3\left(\omega_0^2 - \omega^2 + \frac{4}{t_p^2}\right)\left(\frac{4\omega}{t_p}\right)^2\right].$$

Equations (B.15) and (B.16) give the desired spectral dependence. Figure 4 plots the magnitude of $f(\omega, 0)$.

Appendix C

CONSISTENCY OF HEIGHT GAIN FUNCTION FORMULATIONS AT FLAT PLANE SURFACE

The attenuation function for waves propagating on a rippled surface is given by Hufford [1952] to satisfy

$$W(P) = 1 + \frac{ik}{2\pi}\int da\ \frac{r_0}{r_1 r_2}\ W(Q)\ e^{ik(r_1+r_2-r_0)}\left[\delta + \left(1 + \frac{i}{kr_2}\right)\frac{\partial r_2}{\partial n}\right]. \quad (C.1)$$

When the receiver is above the surface, however, the Hufford treatment gives

$$2W(P) = 1 + \frac{ik}{2\pi}\int da\ \frac{r_0}{r_1 r_2}\ W(Q)\ e^{ik(r_1+r_2-r_0)}\left[\delta + \left(1 + \frac{i}{kr_2}\right)\frac{\partial r_2}{\partial n}\right]. \quad (C.2)$$

Equations (C.1) and (C.2) appear to be identical, except for a factor of 2 in (C.2). Therefore, one would expect that *at the surface of the earth*--i.e., when the elevation above the earth is reduced to zero--the solution of W would depend on which equation one chose to use. Because physical phenomena tend to behave smoothly, however, a 1 m elevation should not significantly change a system with a 3000 m wavelength. Therefore, we look more closely at Eqs. (C.1) and (C.2).

This appendix demonstrates mathematically that the two equations have additional differences, so they actually give a continuous answer at the surface of the earth. Two of the differences are important. First, Eq. (C.1) is an integral *equation* where values of W appearing as the unknown on the left side also appear in the integrand. Equation (C.2) is an integral *formula* where values of W appearing in the integrand are already known from the solution of (C.1). The value of W on the left is not generally from the domain of the integral.

Second, the function $(1/r_2)(\partial r_2/\partial n)$ in both equations is singular at the point where $r_2 = 0$, which can occur only in the case of zero elevation. That term contributes the amount required to maintain

continuity. Since the integrals on a general surface are difficult, we illustrate by considering a plane earth.

On a uniform plane surface, $\partial r_2/\partial n = 0$. Then

$$W(r_0) = 1 + \frac{ik}{2\pi}\int da\ \frac{r_0}{r_1 r_2}\ W(Q)\ e^{ik(r_1+r_2-r_0)}\ \delta\ . \qquad (C.3)$$

We wish to compare this with

$$\lim_{h\to 0} 2W(r_0, h) = \lim_{h\to 0} 1 + \frac{ik}{2\pi}\int da\ \frac{r_0}{r_1 r_2}\ W(Q)\ e^{ik(r_1+r_2-r_0)}\left[\delta + \left(1 + \frac{i}{kr_2}\right)\frac{\partial r_2}{\partial n}\right]. \qquad (C.4)$$

For receivers above a plane earth, $\partial r_2/\partial n = -h/r_2$. Consistency for Eqs. (C.3) and (C.4) would then require

$$\lim_{h\to 0} W(r_0, h) = \frac{ik}{2\pi}\ r_0 \int da\ \frac{W(Q)}{r_1 r_2}\ e^{ik(r_1+r_2-r_0)}\left(1 + \frac{i}{kr_2}\right)\frac{h}{r_2}\ ,$$

where $da = r_2'\, dr_2'\, d\theta_2$, $r_2^2 = r_2'^2 + h^2$, and, in coordinates centered at the observation point P, the integration point Q is at (r_2', θ_2). The following figure shows the relationship between r_0, r_1, r_2', and θ_2:

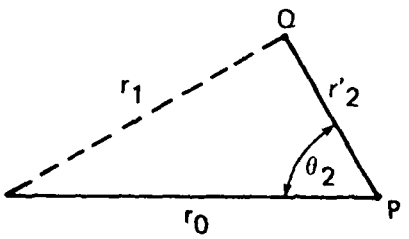

We thus evaluate

$$\lim_{h\to 0} W(r_0, h) = \lim_{h\to 0} \frac{-ik}{2\pi} r_0 \int_0^{\infty}\int_0^{2\pi} r_2' \, dr_2' \, d\theta_2 \, \frac{W(r_2, \theta_2)}{r_1} e^{ik(r_1+r_2'-r_0)} \frac{h}{r_2'^2}$$

$$+ \lim_{h\to 0} \frac{r_0}{2\pi} \int_0^{\infty}\int_0^{2\pi} r_2' \, dr_2' \, d\theta_2 \, \frac{W(r_2, \theta_2)}{r_1} \frac{h}{r_2'^3} . \qquad (C.5)$$

We begin with the first term on the right side of Eq. (C.5). Note that

$$\frac{r_2'h}{r_2'^2} = \frac{r_2'h}{r_2'^2 + h^2}$$

is a function that in the limit $h \to 0$ tends to zero for all $r_2' \neq 0$. For $r_2' \to 0$, the term $(r_2'h)/(r_2'^2 + h^2)$ remains finite, so the entire integral vanishes. The same behavior is shown from a different perspective by regrouping the terms: in the limit $h \to 0$, $h/(r_2'^2 + h^2)$ is a sharply peaked function around $r_2' = 0$. Thus only values of the integrand for $r_2' = 0$ will contribute. But, being proportional to r_2', the integral vanishes.

The remaining term contains the function

$$\frac{r_2'h}{r_2'^3} = \frac{r_2'h}{\left(r_2'^2 + h^2\right)^{3/2}} .$$

This function is also strongly peaked at $r_2' = 0$ in the limit $h \to 0$. However, it becomes large at $r_2' = 0$, so the integral does not vanish. The rest of the integrand will be constant in the infinitesimal interval around $r_2' = 0$. In this case, we have $r_1 = r_0$ and $W(r_2, \theta_2) \to W(r_0)$. Thus

$$\lim_{h\to 0} W(r_0, h) = \lim_{h\to 0} \frac{W(r_0)}{2\pi} \int_0^{2\pi} d\theta \int_0^{\infty} \frac{r_2' h \, dr_2'}{\left(r_2'^2 + h^2\right)^{3/2}} .$$

But

$$\lim_{h\to 0} \int_0^{\infty} \frac{r_2' h \, dr_2'}{\left(r_2'^2 + h^2\right)^{3/2}} = \lim_{h\to 0} \frac{-h}{(r_2'^2 + h^2)^{1/2}} \Bigg|_0^{\infty}$$

$$= \lim_{h\to 0} \left[\frac{-h}{(\infty^2 + 0)^{1/2}} + \frac{h}{(0 + h^2)^{1/2}} \right] \Bigg|$$

$$= 1 .$$

Thus

$$\lim_{h\to 0} W(r_0, h) = W(r_0)$$

and the elevated receiver formula tends to the same value of $h \to 0$ as is given by the equation for the function on the surface.

SYMBOLS

$\vec{A}$ = vector tangent to surface of hill

$\vec{B}$ = vector tangent to surface of hill independent of $\vec{A}$

C = vector normal to $\vec{A}$ and $\vec{B}$

$\vec{E}$ = electric field

$F(t)$ = LORAN signal as function of time

$\vec{H}$ = magnetic field

k = wave number

k_0 = wave number of center component of pulse

$\vec{n}$ = unit normal to ground surface

n_g = index of refraction of ground

t = time

t_f = time of arrival for front of LORAN pulse

t_p = time for LORAN pulse to reach peak

t_3 = time of arrival for third-cycle zero

v = velocity of Gaussian pulse

W = attenuation function for ground wave

$z(x)$ = ground elevation function

δ = skin depth

Δx = width of Gaussian pulse

ε_0 = permittivity of free space

κ = relative permittivity of conductor

μ = permeability

μ_0 = permeability of free space

σ = conductivity

ϕ = phase of W

Φ = ground wave field

Φ_0 = ground wave field if no ground present

ψ = phase of Φ

ω = frequency

ω_0 = center frequency of pulse

MISSION
of
Rome Air Development Center

RADC plans and executes research, development, test and selected acquisition programs in support of Command, Control Communications and Intelligence (C^3I) activities. Technical and engineering support within areas of technical competence is provided to ESD Program Offices (POs) and other ESD elements. The principal technical mission areas are communications, electromagnetic guidance and control, surveillance of ground and aerospace objects, intelligence data collection and handling, information system technology, ionospheric propagation, solid state sciences, microwave physics and electronic reliability, maintainability and compatibility.

Printed by
United States Air Force
Hanscom AFB, Mass. 01731


DA1
FILM